# Feasibility Study of Two Candidate Reaction Wheel/Thruster Hybrid Control Architecture Designs for the Cassini Spacecraft[◊]

**Glenn A. Macala,[1] Allan Y. Lee,[2] and Eric K. Wang[3]**
***Jet Propulsion Laboratory, California Institute of Technology***

As the first spacecraft to achieve orbit at Saturn in 2004, Cassini has collected science data throughout its four-year prime mission (2004–08), and has since been approved for a first and second extended mission through 2017. Cassini carries a set of three "fixed" reaction wheels and a backup reaction wheel (reaction wheel #4) is mounted on top of an articulable platform. If necessary, this platform could be articulated to orient the backup reaction wheel with the degraded wheel. The reaction wheels are used primarily for attitude control when precise and stable pointing of a science instrument such as the narrow angle camera is required. In 2001–02, reaction wheel #3 exhibited signs of bearing cage instability. As a result, reaction wheel #4 was articulated to align with reaction wheel #3. Beginning in July 2003, Cassini was controlled using wheel #1, #2, and #4. From their first use in the spring of 2000 until today, reaction wheels #1 and #2 have accumulated more than 3.5 billions revolutions each. As such, in spite of very carefully management of the wheel spin rates by the mission operation team, there are some observed increases in the drag torque of the wheels' bearings. Hence, the mission operations team must prepare for the contingency scenario in which the reaction wheel #1 (in addition to wheel #3) had degraded. In this hypothetical fault scenario, the two remaining reaction wheels (#2 and #4) will not be able to provide precise and stable three-axis control of the spacecraft. In this study, we evaluate the feasibility of controlling Cassini using the two remaining reaction wheels and four thrusters to meet the science pointing requirements for two key science operational modes: the Optical Remote Sensing and Downlink, Fields, Particles, & Waves operation modes. The performance (e.g., pointing control error, pointing stability, hydrazine consumption rate, etc.) of the hybrid controllers in both operations scenarios will be compared with those achieved using an all-thruster controller design. Strength and weaknesses of the hybrid control architecture are assessed quantitatively.

---

[◊]This paper is dedicated to the loving memory of Mr. William Breckenridge, our mentor, who has contributed to the design of the Cassini hybrid controllers.

[1]Principal engineer, Guidance and Control Section. Division of Autonomous Systems. Mail Stop 198-326, 4800 Oak Grove Drive, Pasadena, CA 91109-8099, USA.

[2]Section Staff, Guidance and Control Section. Division of Autonomous Systems. Mail Stop 230-104, 4800 Oak Grove Drive, Pasadena, CA 91109-8099, USA. Project Element Manager, Cassini Attitude and Articulation Control Mission Operations Team, 1999–2009.

[3]Member of Technical Staff, Guidance and Control Flight Software Validation Section. Division of Autonomous Systems. Mail Stop 230–104, 4800 Oak Grove Drive, Pasadena, CA 91109-8099, USA. Lead engineer, Cassini AACS Flight Software.

## I. Cassini/Huygens Mission to Saturn and Titan

As the first spacecraft (S/C) to achieve orbit at Saturn in 2004, Cassini has collected science data throughout its four-year prime mission, and has since been approved for a first and second extended mission through 2017. The first extended mission is named the Cassini–Equinox mission (from August 2008 to September 2010). It is now in the second extended mission named Cassini–Equinox–Solstice mission (from October 2010 to May 2017). Major science objectives of the Cassini mission include investigations of the configuration and dynamics of Saturn's magnetosphere, the structure and composition of the rings, the characterization of several of Saturn's icy satellites, and Titan's atmosphere constituent abundance. The radar mapper will perform surface imaging and altimetry during many Titan flybys. Doppler tracking experiments using the Earth and the Cassini spacecraft as separated test masses have also been conducted for gravitational wave searches.

Cassini was launched on 15 October 1997 by a Titan 4B launch vehicle. After an interplanetary cruise that lasted almost seven years, on June 30, 2004, Cassini fired one of its two rocket engines for about 96 minutes in order to slow the spacecraft's velocity (by about 626.17 m/s) to allow the spacecraft to be captured by the gravity field of Saturn. This was the most critical engineering event of the entire mission and was executed faultlessly. After the completion of the Saturn Orbit Insertion, Cassini began a complicated suite of orbits about Saturn, designed to optimize science collection over not only Saturn, but also its ice satellites and moons. The orbital tour of Saturn, includes over fifty flybys of Saturn's largest moon, Titan. Titan is the second largest moon in the Solar System, second only to Jupiter's moon Ganymede. However, the exciting discovery of water geysers emanating from Enceladus (in 2005) drove an extensive redesign of the extended mission orbital tour of Saturn.

## II. Spacecraft Configuration[1]

Cassini is perhaps the largest and most sophisticated interplanetary spacecraft humans have ever built and launched. The orbiter is about 6.8 m in height with a "diameter" of 4 meters. The total mass of the spacecraft at launch was approximately 5574 kg, which includes about 3000 kg of bi-propellant, 132 kg of high purity hydrazine, and 2442 kg of "dry" mass. Fig. 1 depicts the cruise configuration of the Cassini spacecraft.

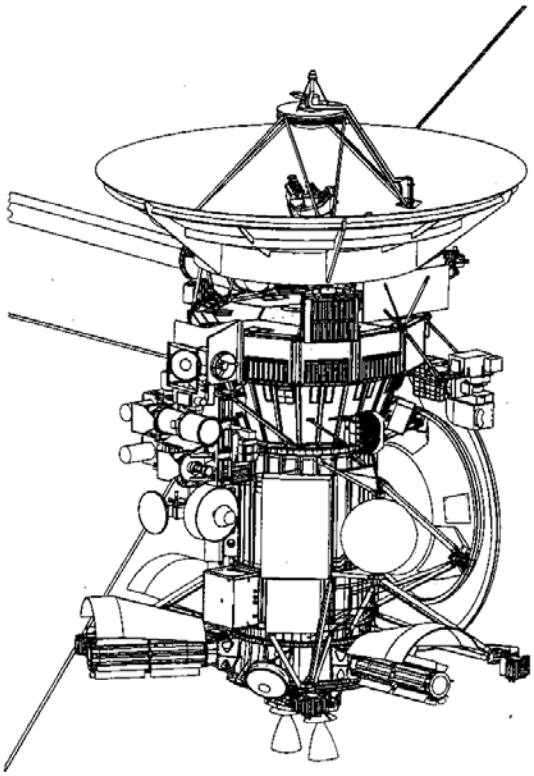

**Fig. 1. Cassini Cruise Configuration**

The base body of the orbiter is a stack consisting of a lower equipment module, a propellant module, an upper equipment module, and a 4-m High Gain Antenna (HGA). The axis of the stack is the Z-axis of the spacecraft. Attached to the stack are the Remote Sensing Pallet and the Fields and Particles Pallet with their scientific instruments. Until separation, the Huygens probe was attached to the base body with its axis of symmetry pointed parallel to the minus X-axis of the spacecraft. The orbiter's 12-bay electronics bus is part of the upper equipment module. An 11-m magnetometer boom is mounted to the upper equipment module. The 4-m parabolic HGA and two Low Gain Antennas (LGAs) are the main communication antennas of the spacecraft. An X-band feed is used for both uplink and downlink communications.

During early Cruise, Cassini used a set of eight Reaction Control System (RCS) thrusters (A-branch) to control the spacecraft's attitude. Thrusters are used to control the spacecraft attitude during low-altitude Titan and Enceladus flybys. During these flybys, Cassini will experience significant atmospheric or plume torque, and only thrusters have the control authority to guarantee spacecraft safety. Fig. 2 (from Reference 1) shows the locations of the four thruster pods that are mounted on a structure that is attached to the lower equipment module. On each one of these pods are mounted two primary thrusters and their "backups." Pointing controls about the S/C's X and Y-axis are performed using four Z-facing thrusters. Controls about the Z-axis are performed using four Y-facing thrusters. Since the spring of 2009, Cassini has been using the B-branch thrusters for attitude control.[2] For the B-branch thrusters, the distance between thruster pods 1 and 2 (or between thruster pods 3 and 4) is ≈2×1.234 = 2.468 m. The distance between thruster pods 1 and 4 (or between thruster pods 2 and 3) is ≈2×1.610 = 3.22 m. Cassini's thrusters have rich heritage from the Voyager program.

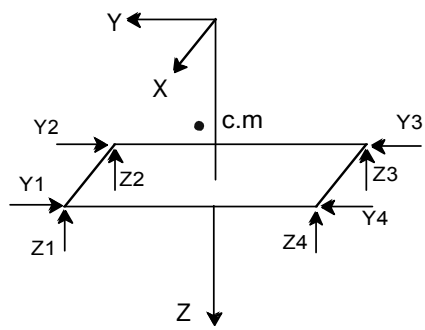


**Fig. 2. Cassini Thruster Pod Location**

With reference to Fig. 2, we see that to slew about the positive Z-axis of the spacecraft, one must fire both the $Y_2$ and $Y_4$ thrusters simultaneously. Thrusts generated by these firings will almost cancel each other, and the ΔV imparted on the spacecraft will be quite small. Similarly, to slew about the negative Z-axis of the spacecraft, one must fire both the $Y_1$ and $Y_3$ thrusters simultaneously. Again, the ΔV imparted on the spacecraft will be small. On the other hand, a slew about either the ±X-axis or ±Y-axis will involve firings of the Z-facing thrusters. Since these Z-facing thrusters all point in the same direction, slewing the spacecraft about either the X or Y-axis will generate unwanted ΔV on the spacecraft that must be predicted and incorporated into the design of the spacecraft trajectory design. For this reason, during Tour, the spacecraft was slewed using three prime reaction wheels.

Cassini carries a set of three "strap-down" reaction wheels that are mounted on the lower equipment module. The Reaction Wheel Assemblies (RWAs) are used primarily for attitude control when precise and stable pointing of a science instrument such as the narrow angle camera is required. The obvious merits of using reaction wheels over thrusters are the absence of unwanted ΔV imparted on the spacecraft and the conservation of hydrazine.

The wheels are oriented "equal distance" from the spacecraft's Z-axis. That is, the angle between any of these three RWA's angular momentum vector and the spacecraft's Z-axis is $\cos^{-1}(1/\sqrt{3}) = 54.7356°$. A backup reaction wheel is mounted on top of an articulable platform. If necessary, this platform could be articulated to orient the backup reaction wheel (wheel #4) with a degraded wheel. Fig. 3 (from Ref. 3) depicts the orientations of the four reaction wheels relative to the spacecraft's coordinate frame at Launch. At Launch, the backup reaction wheel is mounted parallel to reaction wheel #1. On July 11, 2003, the platform was articulated in order to align the backup reaction wheel with reaction wheel #3. Since late 2000, the ball bearings of reaction wheel #3 had exhibited signs of cage instability.[1,4] A decision was made to replace it by the backup wheel.[1]

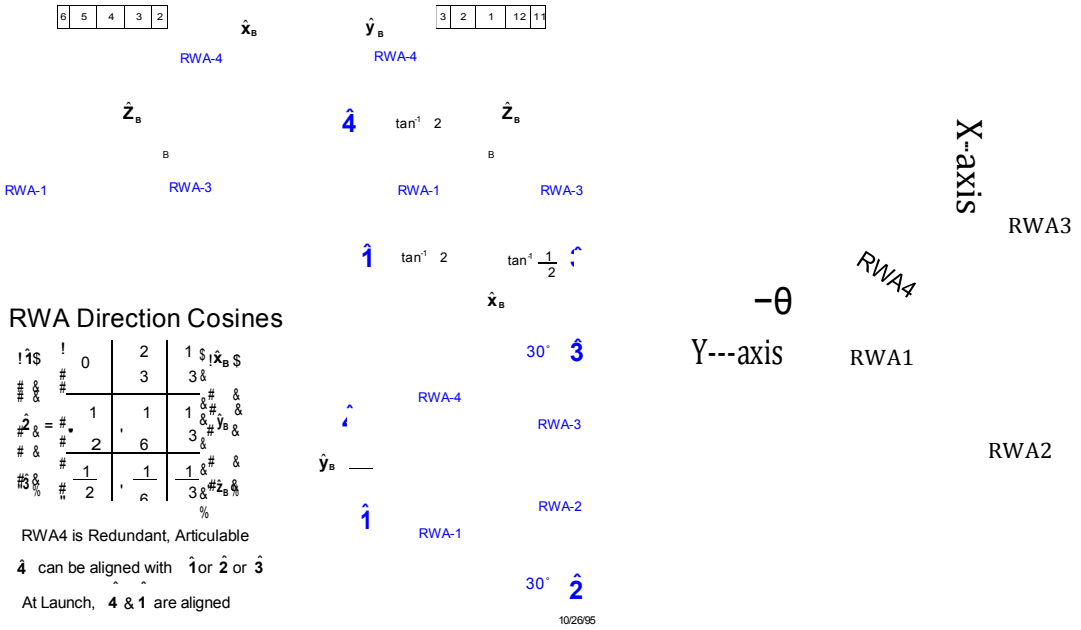


**Fig. 3 Cassini Reaction Wheel Orientation**

Cassini carries twelve scientific instruments.[5] Six of the instruments measure properties of objects remote from the spacecraft. These remote sensing instruments are:

1. Imaging Science Subsystem (ISS),
2. Visible and Infrared Mapping Spectrometer (VIMS),
3. Composite Infrared Spectrometer (CIRS),
4. Ultraviolet Imaging Spectrograph (UVIS),
5. Cassini Radar (RADAR), and
6. Radio Science Subsystem (RSS).

The first four of these instruments are mounted and co-aligned on the remote sensing pallet, which in turn is mounted on the upper equipment module (see Fig. 1). Also mounted on the remote sensing pallet are two redundant stellar reference units (star trackers). The ISS consists of two cameras: Narrow Angle Camera (NAC) and the Wide Angle Camera (WAC). These science instruments must be operated only when the spacecraft has achieved a high level of pointing stability. The needed pointing stability could only be achieved when the spacecraft is controlled by the reaction wheels.[6] RADAR is designed for observation of the surface of Titan during close flybys of the satellite. Radio science measurements will provide data on the atmospheres and ionospheres of Saturn and Titan, on the rings, and on the gravity field of Saturn.

In addition to the remote sensing instruments, Cassini also carries six instruments that observe fields, particles, and plasma waves. These instruments are:

1. Dual technique magnetometer (MAG),
2. Radio and Plasma Wave Science (RPWS),
3. Cassini Plasma Spectrometer (CAPS),
4. Magnetospheric Imaging Instrument (MIMI),
5. Cosmic Dust Analyzer (CDA), and
6. Ion and Neutral Mass spectrometer (INMS).

These instruments are located on various parts of the orbiter as indicated in Fig. 1. Details of these instruments are given in Ref. 5. The Huygens probe, designed and built by ESA, also carried six science instruments. Detailed descriptions of these Huygens instruments are given in Ref. 5.

To meet the science needs of these 12 science instruments, the Cassini mission operations team divides the 24-hour cycle into two distinct operation segments: 15 hours in the Optical Remote Sensing (ORS) mode and 9 hours in the Downlink, Fields, Particles, and Wave (DFPW) mode. In the ORS mode, the spacecraft is slewed using the RWA's in order to point the optical bore-sight vectors of four instruments (for example, NAC, whose bore-sight vector is aligned with the spacecraft's -Y-axis) to the inertial targets of interest. The inertial pointing control requirement for science observations made using these remote-sensing instruments is 2 mrad (X and Z-axis, radial 99%).[1] At the same time, the point stability of the spacecraft must meet requirements specified in Refs. 1 and 6.

In the DFPW mode, the HGA axis is pointed at Earth with an inertial pointing control requirement of 3.14 mrad (X and Y-axis, radial 99%).[1] With this HGA-to-Earth attitude, ground-based commands could be sent to the spacecraft while at the same time telemetry data are transmitted from the spacecraft. At the same time, without changing this HGA-to-Earth attitude, the spacecraft is commanded to spin about the Z-axis at a constant spin rate that is command-able. A representative spin rate is 3.1 mrad/s. With this spin rate, the six Fields, Particles, and Plasma Waves instruments collect science data as they scan the 360° sky.

## III. Attitude and Articulation Control System

Perhaps no other spacecraft subsystem must satisfy as many science and mission requirements as the Attitude and Articulation Control Subsystem (AACS). The Cassini AACS estimates and controls the attitude of the three-axis stabilized Cassini spacecraft. It responds to ground-commanded pointing goals for the spacecraft's science instruments and communication antennas with respect to targets of interest. The AACS also executes ground-commanded spacecraft velocity changes. To this end, AACS uses either a rocket engine or a set of Z-facing thrusters to effect a velocity change. Accuracy requirements for these propulsive maneuver executions are given in Ref. 1.

Cassini is a three-axis stabilized spacecraft. Three-axis stabilized spacecraft are best suited to missions where fine resolution imaging science and a high degree of maneuverability are required. AACS equipment use by Cassini include two star trackers (prime and backup), two four-axis inertial reference units (prime and backup), two two-axis Sun sensors (prime and backup), one single-axis accelerometer (with an "analytical" backup), four reaction wheels (see Fig. 3), eight hydrazine thrusters (and their backup counterparts, see Fig. 2), two sets of two-dof engine gimbal actuators (for two 445-N engines), and two flight computers (prime and backup). The locations of the Cassini AACS equipment are given in Ref. 1.

During early cruise, Cassini used a set of eight thrusters to maintain three-axis attitude control of the spacecraft. The thruster configuration is depicted in Fig. 2. A conventional Bang-Off-Bang (BOB) thruster control algorithm is used by Cassini AACS. The BOB algorithm uses error signals that are the weighted sums of per-axis attitude errors and attitude rate errors to control thruster firings.

The Reaction Wheel Assemblies (RWAs) are used primarily for attitude control when precise and stable pointing of a science instrument (such as NAC) is required during the prime mission phase. To this end, RWAs are used to slew the spacecraft from one attitude to another, rest to rest. Once it has arrived at the targeted attitude, the NAC "stares" at the target for a period of time during which the spacecraft attitude must be stable. The RWA-based pointing stability flight performance of the Cassini spacecraft is given in Ref. 6.

## IV. Reaction Wheel Operational Constraints

The use of reaction wheels is subjected to multiple constraints. Firstly, at no time should one allow the spin rates of any of the three prime reaction wheels to exceed the momentum storage capacity (about ±2000 rpm, which corresponds to a peak momentum storage capacity of 34 Nms) of the wheels. In the current Cassini Fault Protection (FP) design, such a violation will trigger a transition from reaction wheel control to thruster control. Secondly, the total number of revolutions of the three prime wheels that is incurred as a result of science slews must be kept as low as possible. This is so because the health state of RWA is related to the accumulated revolutions of the wheels. These two constraints discourage high-speed wheel operations. However, the operation hours the wheels spent inside a "low-rpm" region must also be minimized. This is the case because when a wheel spin rate falls below a threshold, the thickness of the lubrication film (between the balls, the races, and the cage) might be smaller than the root-mean-square value of the surface roughness of the bearing balls and races. As such, there will be metal-to-metal contact between the balls and the races. The wheels are said to operate in a sub-EHD state (EHD = Elasto-Hydro-Dynamic). This is highly undesirable because of the resultant lubricant degradation.

However, it is very difficult to avoid operating the wheels inside the "low-rpm" region during both the ORS and DPFW modes. This is so because the momentum storage capacity of the wheels (≈34 Nms) is small when compared with the large moments of inertia of Cassini. For example, when the S/C is slewed about the X-axis at a rate of 1.9 mrad/s, the angular momentum "delta" is 7,403×1.9e-3≈ 14.1 Nms. This represents a significant percentage of the wheels' capacity about the X-axis. Obviously, the wheel rate at the start of this slew must be carefully managed. Else, the peak rates of wheels at the end of the slew might exceed the 2000-rpm limit. For Cassini mission operations, the management of the RWA rates, from RWA momentum bias to bias, is performed using a Ground Software (GSW) tool named RBOT (Reaction Wheel Bias Optimization Tool).[4]

In RBOT, the optimal selection of RWA momentum bias for performing long periods of spacecraft slews on reaction wheels is formulated as an optimization problem. The cost functional to minimize includes terms that are related to reaction wheel consumables (wheel revolutions and dwell time inside the low-rpm region) and the momentum storage capacity of the reaction wheels. The formulated optimization problem is solved using a direct search numerical method. A novel computational efficient formulation and gain table schemes are implemented to find the solution rapidly and robustly.[4] Effectiveness of this GSW tool has been demonstrated via years of flight experience.

But, in spite of very carefully management of the reaction wheel spin rates by the mission operations team, in 2001–02, reaction wheel #3 began showing signs of bearing cage instability. Bearing cage instability is an "uncontrolled" vibration of the bearing cage that can produce high impact forces internal to the bearing. Bearing cage instability has been known to negatively impact the health of the bearing in past missions.[7] As a result, on July 16, 2003, the articulable wheel #4 was articulated to the orientation of reaction wheel #3.[1] Thereafter, the spacecraft was controlled using wheel #1, #2, and #4.

With the passage of time, the large number of wheel revolutions accumulated on the wheels has led to some observed increase in the drag torque of the wheels' bearings. The long-term trends of the viscous coefficients of the wheels' bearings were documented in Ref. 1. In particular, the viscous coefficients of two of the three strapped-down wheels, reaction wheels #1 and #3, had attained levels that are significantly higher than their pre-launch values. Hence, the mission operations team must prepare for a contingency scenario in which these two reaction wheels have failed. In this *hypothetical* fault scenario, the two remaining healthy wheels, RWA-2 and RWA-4, will not be able to provide accurate and stable three-axis control of the spacecraft. In this study, we research the feasibility of using two hybrid controllers (each uses two reaction wheels and four thrusters) to meet the science and HGA pointing requirements in two key Cassini operational modes.

## VI. Two Candidate Hybrid Control Architecture Designs

Cassini operational mode, or "opmode", represents a predefined set of allowable spacecraft configurations that ensure the flight system is operated within specified power margins. Opmodes constrain the power consumption of the spacecraft, not the telemetry rate or the S/C's attitude, and define the maximum power consumption allowed for each instrument and subsystem. Cassini has four categories of opmodes; Downlink Fields Particles & Waves (DFPW), Optical Remote Sensing (ORS), Radar, and Radio Science Subsystem (RSS). Two candidate hybrid control architecture designs are proposed for the ORS and DFPW opmodes in which the precise and stable pointing control of either science instruments or the HGA is of critical importance. Low-altitude Radar observations of Titan were performed using RCS thrusters. Only thrusters can generate the needed control authority to overcome the atmospheric torque imparted on the spacecraft due to the substantial Titan atmosphere. Hence, RCS thrusters will continue to be used for most of these observations in the Radar opmode. The pointing needs of the RSS opmode are very similar to that of the DFPW opmode. Hence, the DFPW hybrid controller will also be used for the RSS opmode.

In the ORS mode, both the pointing control and pointing stability requirements about the spacecraft's X and Z-axis are stringent. Hence, it made sense to use the two reaction wheels to perform attitude control about these two axes while the Y-axis is controlled via four Z-facing thrusters (see Fig. 2). Details associated with the ORS hybrid controller are given in Section VII.

In the DFPW mode, the HGA pointing control requirement about the spacecraft's X and Y-axis are stringent. Hence, it made sense to use the two reaction wheels to perform attitude control about these two axes while the Z-axis is controlled using the Y-facing thruster couples (see Fig. 1). Thrusts generated by these thruster couples ($Y_1$ & $Y_3$, and $Y_2$ & $Y_4$) will almost exactly cancel each other, and the $\Delta V$ imparted on the spacecraft will be small. However, rotating the S/C (about its Z-axis) with spinning wheels will generate a gyroscopic torque vector. The resultant firings of Y-facing thrusters will waste hydrazine. These are obvious merits and demerits of this hybrid controller architecture. Details associated with the DFPW hybrid controller are given in Section VIII.

## VII. Candidate Hybrid Control Architecture for the ORS Operations Mode

Since wheel #4 is mounted on an articulable platform, we should take advantage of this "degree of freedom" and articulate it to an orientation such that that wheel #2 and the (articulated) #4 can best control the spacecraft's X and Z-axis. In our study, the criterion we used to pick the best orientation for wheel #4 is to minimize the "cross-couplings" between the X-to-Y and Z-to-Y axes. In this configuration, attitude commands about the X-axis (and Z-axis) will produce acceptably small un-wanted motion about the Y-axis. Frequent thrusters' firing will then not be needed to maintain the spacecraft's Y-axis attitude.

Let $-\theta$ be the angle between the S/C's +Y-axis and the projection of the wheel #4 orientation on the X-Y plane of the spacecraft as depicted in Fig. 3. Using the direction cosine matrix between the reaction wheels and the spacecraft's axes depicted in Fig. 3, we have:

$$\begin{bmatrix} T_X \\ T_Y \\ T_Z \end{bmatrix} = \begin{bmatrix} -1/\sqrt{2} & -\sqrt{2/3}\sin\theta \\ -1/\sqrt{6} & +\sqrt{2/3}\cos\theta \\ +1/\sqrt{3} & +1/\sqrt{3} \end{bmatrix} \begin{bmatrix} T_2 \\ T_4 \end{bmatrix}, \qquad A = \begin{bmatrix} -1/\sqrt{2} & -\sqrt{2/3}\sin\theta \\ +1/\sqrt{3} & +1/\sqrt{3} \end{bmatrix} \tag{1}$$

where A is the 2×2 mapping matrix between wheel 2/4 and the spacecraft's X/Z axes. It is formed using the first and third rows of the 3×2 matrix given in Eq. (1). Let $[T_x\ T_z]^T$ be the [X, Z] torque command vector that is needed by the RWA controller. To generate this torque vector using reaction wheel #2 and #4, one can use the "pseudo inverse" of the mapping matrix A:

$$\begin{bmatrix} T_2 \\ T_4 \end{bmatrix} = [A^T A]^{-1} A^T \begin{bmatrix} T_X \\ T_Z \end{bmatrix} \tag{2}$$

If the desired torque is about the X-axis, then, substitution of $[T_x\ T_z]^T = [1, 0]^T$ into Eq. (2), and then back substitution of the resultant $[T_2\ T_4]^T$ into Eq. (1) give:

$$\begin{bmatrix} T_X \\ T_Y \\ T_Z \end{bmatrix} = \begin{bmatrix} +1 \\ \frac{1}{18}(\sqrt{3}-2\sin\theta)(1+2\cos\theta)/\Delta \\ 0 \end{bmatrix}, \tag{3}$$

$$\Delta = \frac{1}{6} + \frac{2}{9}\sin^2\theta - \frac{2}{3\sqrt{3}}\sin\theta$$

Note that, the desired X and Z-axis torque commands are achieved <u>exactly</u> but there is an unwanted coupling torque generated about the Y-axis. Similarly, if the desired torque is about the Z-axis, substitution of $[T_x\ T_z]^T = [0, 1]^T$ into Eq. (2), and then back substitution of the resultant $[T_2\ T_4]^T$ into Eq. (1) give:

$$\begin{bmatrix} T_X \\ T_Y \\ T_Z \end{bmatrix} = \begin{bmatrix} 0 \\ \frac{1}{9\sqrt{2}}(\sqrt{3}-2\sin\theta)(\sin\theta+\sqrt{3}\cos\theta)/\Delta \\ +1 \end{bmatrix}, \tag{4}$$

Again, there is an unwanted coupling torque generated about the Y-axis. Note from Eq. (3) that $\Delta$ becomes zero when $\theta = +60^\circ$ or $+120^\circ$. At these angles, the numerators of the two $T_Y$ terms in Eqs. (3–4) also become zero. But, in the limit, the coupling coupling terms become *infinity*. With either of these articulation angles, the rank of the matrix "A" in Eq. (1) becomes 1. As such, control of S/C's X and Z could not be performed using RWA-2 and RWA-4 (in this articulated position). These angles are to be avoided.

The angle $\theta_{optimal}$ that minimizes the Root-Sum-of-Squares (RSS) of the two Y-axis coupling torque represents a candidate orientation of the articulable wheel. Fig. 4 depicts the variation of the RSS torque about the Y-axis with $\theta$. From Fig. 4, the optimal angle is about $-81.8^\circ$, and the corresponding RSS value is 0.4472 units. With this $\theta_{optimal}$, the magnitudes of the Y-axis coupling torque due to one unit of X-axis and Y-axis torque command are +0.346 and -0.283 units, respectively. If we select $\theta$ to be $-84.7^\circ$, the two coupling terms will be almost identical (+0.318 and -0.317 units for one unit of X-axis and Y-axis torque command, respectively). The corresponding RSS value is 0.4494 units (only about 0.5% larger than the optimal value).

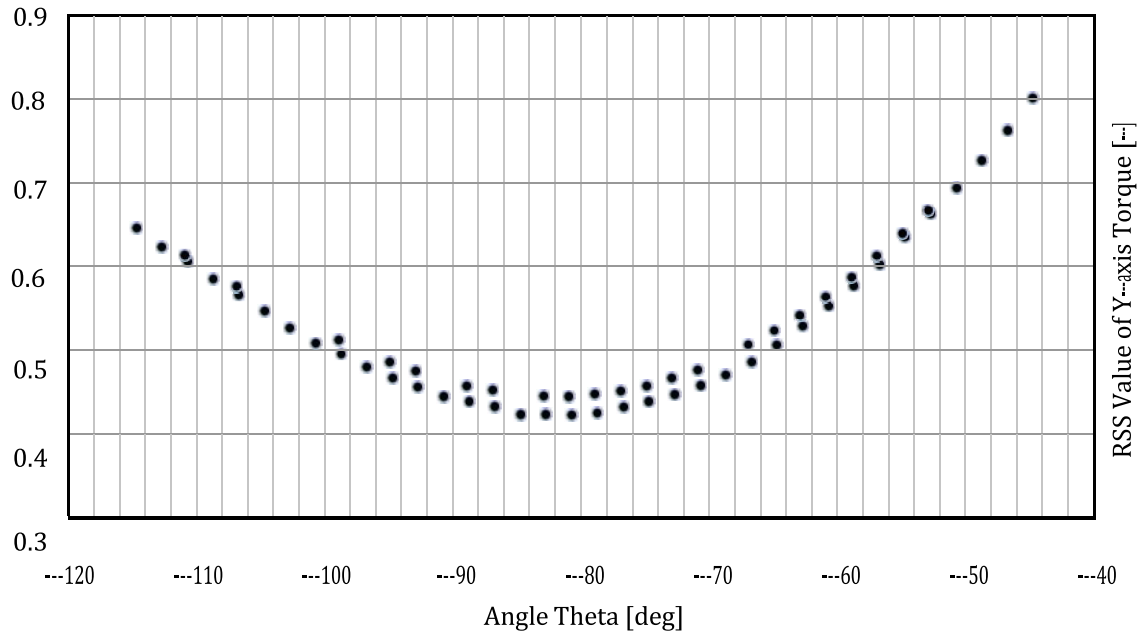


**Fig. 4. Best Torque-based Orientation of the Articulable Reaction Wheel**

The design of the Cassini RWA attitude control system is described in Ref. 3. As explained in that reference, to realize a change in the spacecraft's attitude about $i^{th}$ axis (i = X, Y, and Z-axis), the RWA controller computes and outputs the needed $i^{th}$ axis acceleration command. Next, the acceleration command is multiplied by the S/C's inertia tensor in order to compute the required accelerating torque command. That is, it is the acceleration command (instead of the torque command) that is the fundamental quantity of importance. For one unit of commanded X-axis acceleration, the unwanted coupling acceleration generated about the Y-axis is given by element [2,1] of the matrix given in Eq. (3) times $I_{XX}/I_{YY}$. Similarly, for one unit of Z-axis acceleration, the unwanted coupling acceleration generated about the Y-axis is given by element [2,1] of the matrix given in Eq. (4) times $I_{ZZ}/I_{YY}$. The angle $\theta_{optimal}$ that minimizes the RSS of these two coupling Y-axis accelerations represents the best orientation of the articulable wheel. From Fig. 5, the optimal angle is about –99.6˚, and the corresponding RSS value is 0.3856 units. With this $\theta_{optimal}$, the magnitudes of the Y-axis coupling acceleration due to one unit of X-axis and Z-axis command accelerations are +0.2188 and -0.3175 units, respectively. If we select $\theta_{optimal}$ to be –94.2˚, the RSS value is 0.3937 units (only about 2.1% larger than the optimal value). But with this angle, the magnitudes of the Y-axis coupling accelerations due to one unit of X-axis and Y-axis command accelerations are +0.2785 and -0.2783 units, respectively. Note that the magnitudes of these coupling Y-axis accelerations are almost identical. This is the angle selected for the ORS hybrid controller.

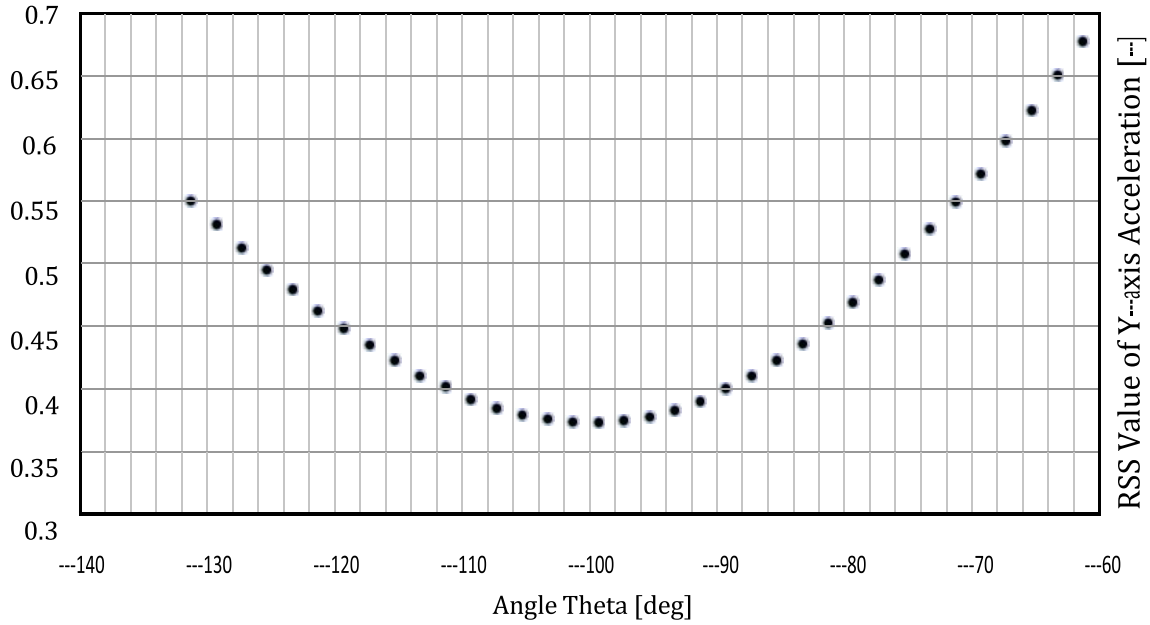


**Fig. 5. Best Acceleration-based Orientation of the Articulable Reaction Wheel**

With the ORS hybrid controller, when Z-facing thrusters are fired to overcome the Y-axis coupling torque, they will generate disturbance torque about the S/C's X-axis. This is an obvious weakness because the S/C's X-axis must be kept as stable as possible. There will be no disturbance torque about the spacecraft's Z-axis because Z-facing thrusters could not generate a torque about the Z-axis. The resultant X-axis disturbance torque will have to be removed using reaction wheels #2 and #4. Accordingly, some of the control authority of the reaction wheel pair must be allocated to fight the X-axis disturbance torque. The coupling between the RWA-controlled X and Z-axis, and the RCS-controlled Y-axis is hard to analyze analytically. In this study, we use a test bed to evaluate the performance of the ORS hybrid controller.

The performance of the ORS hybrid controller is evaluated using a CIRS science observation sequence performed on 2011-346T07:18. The Cassini Composite Infrared Spectrometer (CIRS) consists of two spectrometers (far-Infrared and mid-Infrared). The bore-sight axis of CIRS is aligned with the S/C's –Y-axis, and the diameter of the CIRS focal plane #1 is 3.9 mrads. In this particular observation sequence, the CIRS focal plane #1 was pointed at Dione with the following sequence of incremental steps (unit of angular displacements is mrads. See Fig. 6): $[\Delta ß_X, \Delta ß_Z]$: From [0, 0] to [-14.189,0], to [0,-1.726], to [+14.189,0], to [0,-1.726], and repeated. The RWA-based X-axis and Z-axis slew acceleration limits are 5e-3 and 10e-3 mrad/s$^2$, respectively. The time histories of the resultant spacecraft's acceleration, rate, and displacement commands for both the X and Z-axis are given in Fig. 7. The time it takes to complete a 14.189-mrad X-axis slew is $2\sqrt{(14.189/0.005)} \approx 106.54$ s. The time it takes to complete a 1.726-mrad Z-axis slew is $2\sqrt{(1.726/0.01)} \approx 26.28$ s. Note that a settling time of ≈ 4.5 s is used in between successive slews. The CIRS team uses these types of observations for composition and thermal mapping of Dione. Similar observations have led to the discovery of geysers near the South pole of Enceladus.[9] Values of key parameters of the simulated spacecraft system are summarized in Table 1.

The per-axis spacecraft's rates achieved by the ORS hybrid controller are depicted in Fig. 8. Note that, both the X and Z-axis spacecraft rate commands are achieved closely but there is an unwanted Y-axis rate that is generated as a result of the X/Y and Z/Y couplings.

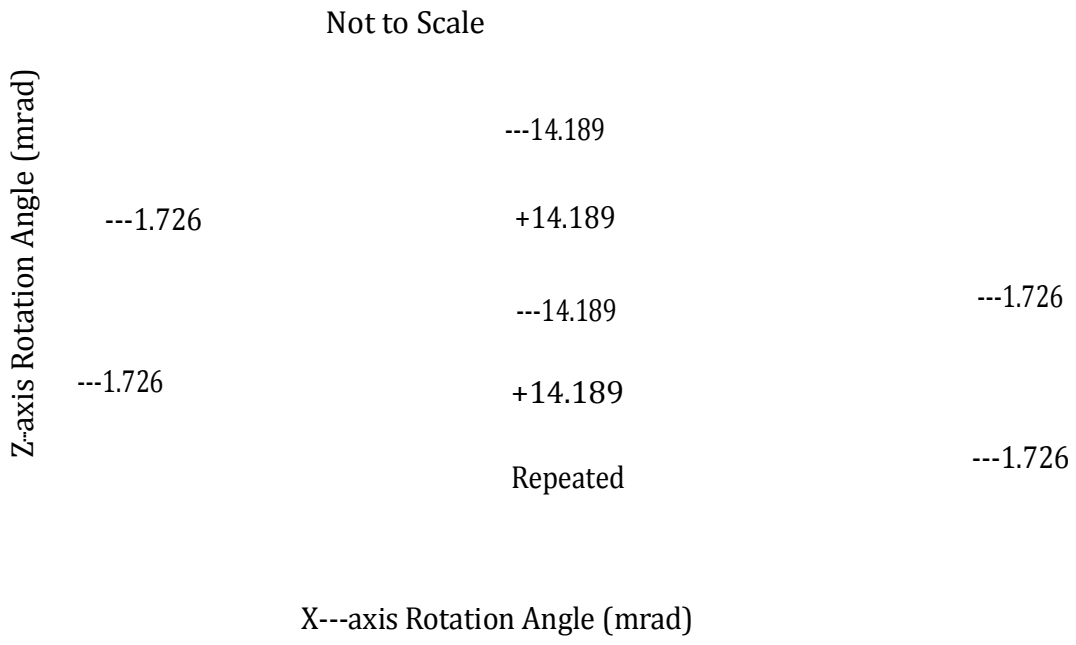


**Fig. 6. CIRS Observation of Dione on DOY 2011-346**

**Table 1. Values of Key Spacecraft and CIRS Sequence Parameters**

| Parameter | Units | X-axis | Y-axis | Z-axis |
|---|---|---|---|---|
| Moment of Inertia | kg-m$^2$ | 6558 | 5393 | 3518 |
| Profile Rate | mrad/s | 1.8 | 0.89 | 3.8 |
| Profile acceleration | mrad/s$^2$ | 0.005 | 0.005 | 0.010 |
| c.m. location | m | +0.13 | +0.057 | +1.064 |
| Mass | kg | | 2292.2 | |
| Thruster's mag. | N | | 0.676 | |
| Thruster Specific Impulse (5% duty cycle) | s | | 180 | |
| Articulation angle | deg | | -94.2 | |

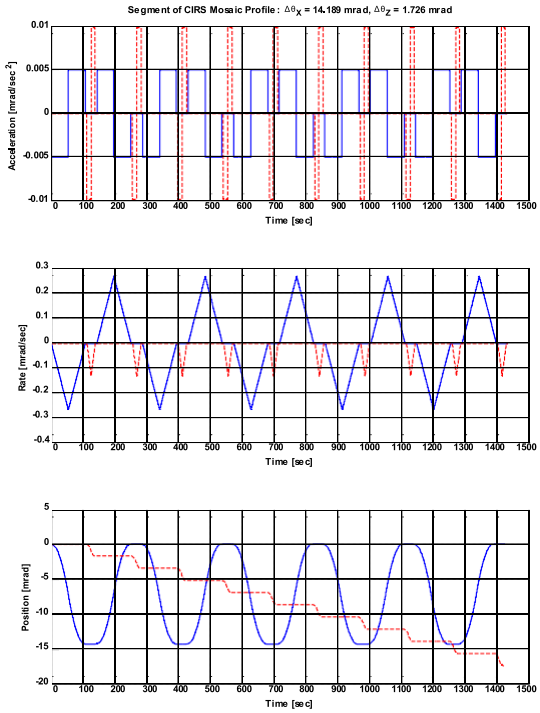


**Fig. 7. X and Z-axis Acceleration, Rate, and Displacement Commands for The CIRS Science Sequence (X-axis: Solid Blue, Z-axis: Dashed Red)**

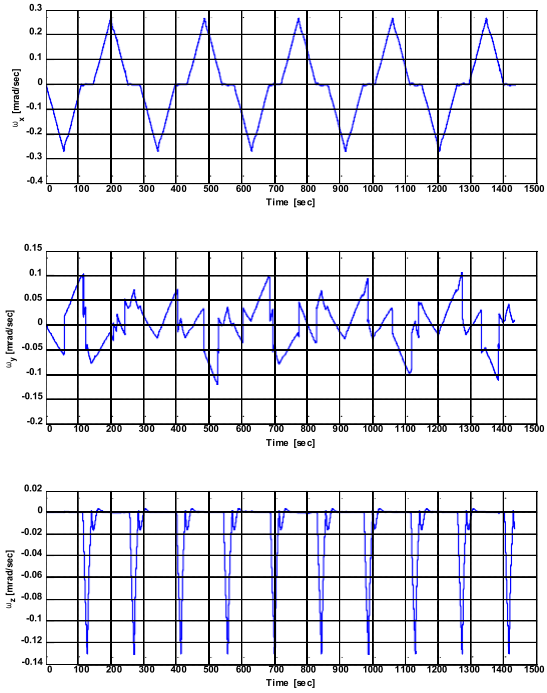


**Fig. 8. Per-axis Spacecraft Rate Achieved by the ORS Hybrid Controller**

The attitude control performance of the ORS hybrid controller is depicted in Fig. 9. Both the X and Z-axis attitude of spacecraft is controlled by the reaction wheels. Hence, not surprisingly, the attitude control errors about these axes are very small, on the order of ±0.1 mrads. This level of attitude control error is consistent with that achieved when Cassini was controlled by three wheels.[1] With these X and Z-axis attitude control errors, the inertial pointing control requirement for ORS science instruments, 2 mrad (X and Z-axis, radial 99%), could be met with margin.[6] From Eqs. (3)–(4), we note that X-axis and Z-axis RWA torque commands will produce unwanted coupling torque about the S/C's Y-axis. Hence, the Y-axis attitude control error will traverse back and forth between the selected dead-band limits (of ±2 mrads). This should not be a problem because the spacecraft's Y-axis is nearly aligned with the "twist" axis of all the ORS instruments.

The attitude rate control performance of the ORS hybrid controller is depicted in Fig. 10. The "instantaneous line-of-sight angular rates" about the S/C's X and Z-axis are bounded by ±10 and ±20 μrad/s, respectively. The Z-axis Moment of Inertia (MOI) of the spacecraft is about a factor of 1.9 smaller than its X-axis counterpart (see Table 1). Hence, not surprisingly, the peak Z-axis angular rate is about a factor of two larger than its X-axis counterpart. The pointing stability requirements for CIRS observations are 36 and 100 μrad for exposure times of 5 and 22 s, respectively ($2\sigma$ per axis).[6] The corresponding $2\sigma$ "instantaneous line-of-sight angular rate" requirements are 4.5–7.2 μrad/s (the corresponding $3\sigma$ requirements are 6.8–10.8 μrad/s). However, these pointing stability requirements are only applicable when the spacecraft is in a quiescent state (all per-axis rate ≤ 0.01 °/s). The X/Z-axis pointing stability achieved by the ORS hybrid controller approaches these requirements even when the S/C was being slewed.

For this particular 1420-s CIRS mosaic sequence, the estimated on-time's of the [$Z_1$, $Z_2$, $Z_3$, $Z_4$] thrusters are depicted in Fig. 11. The total on-time of these four Z-facing thrusters is 10.8 s. Hence, the hydrazine consumption rate is on the order of 0.676×10.8/(180×9.806)/(1420/3600) = 10.5 grams per hour (4.14 grams for the 1420-sec CIRS mosaic sequence). This hydrazine consumption could be reduced if smaller X and Z-axis angular acceleration limits are used to execute the CIRS mosaic slews. But this will be at the expense of a longer slew time. Also, if the "two-sided" Y-axis dead-band motion could be made "one-sided" via the tuning of RCS controller parameters (see, e.g., the flight-proven technique described in Ref. 1), we might be able to achieve more hydrazine saving.

An upper bound on the total hydrazine mass consumed could be derived via first principle:

$$M_{Total} = \frac{2 I_{YY}}{I_{SP} L} \{ N_X \sqrt{\alpha_X \theta_X} + N_Z \sqrt{\alpha_Z \theta_Z} \} \tag{5}$$

This equation gives the dependency of the hydrazine cost of the mosaic sequence on the per-axis angular accelerations, the per-axis step sizes, and the cross coupling factor $\beta$. The Y-axis moment of inertia ($I_{YY}$, in kg-m$^2$) and the X and Z-axis angular accelerations ($\alpha_X$ and $\alpha_Z$, in rad/s$^2$) are given in Table 1. The X and Z-axis slew angle steps are: $\theta_X$ = 14.189 mrad, and $\theta_Z$ = 1.726 mrad. The number of X and Z-axis steps in the CIRS mosaic are: $N_X = N_Z = 10$. The moment arm L = 1.234 m, and the specific impulse of hydrazine is $I_{SP}$ = 180!9.806 ≈ 1765.1 Ns/kg. The cross coupling factor between X and Y-axis acceleration (which approximates the cross coupling between the Z and Y-axis acceleration) is $\beta$ = 0.2785 (see Section VII). The resultant upper bound on the total hydrazine mass is 5.48 gram, which is larger than the computed fuel cost (4.14 grams).

The magnitude of the ΔV generated by thrusters' firing is depicted in Fig. 12. The thrusters that are used by the ORS hybrid controller are nearly aligned with the S/C's Z-axis. Hence, the Z-axis component of the ΔV vector is the largest (≈ -3.15 mm/s). Note that this ΔV magnitude is consistent with the 10.8 s total thrusters' on-time depicted in Fig. 11. This is the case because 2292.2 kg×3.15e-3 m/s/0.676 N ≈ 10.7 s. During the slews, the spacecraft's attitude is being changed 14.189 mrads about X-axis, back and forth, so on average the X-axis attitude is about -7.1 mrad from the initial attitude. Hence, the Y-axis component of ΔV is 3.15×sin(-0.007.1)≈-0.022 mm/s, which is close to that depicted in Fig. 12. During the slews, we are also moving the S/C's Z-axis from 0 to -17.26 mrads (in ten steps of -1.726 mrads each). Hence, the X-axis ΔV is about -0.022×sin(-0.01726) ≈ +3.8e-4 mm/s (see also Fig. 12).

Without the hybrid controller, and with failed RWA-1 and RWA-3, the CIRS mosaic sequence could only be performed using an all-thruster control system. The performance of the all-thruster system is evaluated using the Flight Software Development System (FSDS). The test bed FSDS was created to support the validation of flight software (FSW) in the Cassini attitude control environment.[8] Detailed performance of the all-thruster controller is given in Appendix A. In Table 2, the performance of the all-thruster controller is compared with that of the ORS hybrid controller. Note that both the X/Z-axis attitude control errors and the instantaneous line-of-sight angular rates of the all-thruster controller are at least one order of magnitude worst than their counterparts (achieved by the hybrid controller). Also, both the hydrazine consumption rate and the ΔV generated using the all-thruster control system are a factor of 3.5 worst than their counterparts generated using the hybrid controller. The merit of the hybrid controller is clearly exhibited in Table 2.

**Table 2. Figures of Merit: ORS Hybrid Controller vs. All-thruster Controller**

| Figures of Merit | Units | ORS Hybrid Controller | All-thruster Controller† |
|---|---|---|---|
| Peak Attitude Control Error: | | | |
| X-axis | mrads | ±0.07 | ±2.0 |
| Z-axis | mrads | ±0.10 | ±2.0 |
| Peak Instantaneous Line-of-Sight Rate: | | | |
| X-xis | mrad/s | ±0.011 | ±0.19 |
| Z-axis | mrad/s | ±0.020 | ±0.14 |
| Hydrazine Consumption Rate | gram/hr | 10.6 | 36.9 |
| Total ΔV magnitude generated at end of mosaic (Y-axis dead-band =2 mrads) | mm/s | 3.15 | 11.3 |

†With per-axis attitude controller dead-band of [2,2,2] mrads.

Large angle rotations about either the X or Z-axis made using this ORS hybrid controller are problematic. A rotation about the X-axis (Z-axis) will lead to a growth in Z-axis (X-axis) angular momentum. Fig. 13 depicts the time histories of the per-axis angular momenta of the reaction wheels. Note that the X-axis (Z-axis) angular momentum change is related to the Z-axis (X-axis) angular displacement depicted in Fig. 7. On the other hand, the Y-axis angular momentum simply fluctuates about a mean value. When absorbed by the two reaction wheels, these "delta" angular momenta will cause the wheels' rates to increase with the slew angle. Ultimately, the angular momentum capacity of one or both wheels will be exceeded. In the DFPW operations mode, the spacecraft is often time commanded to spin continuously about the S/C's Z-axis. The Z-axis rotation angle could be as large as 14 revolutions. As such, the ORS hybrid controller could not support the science needs of the DFPW mode. A new hybrid controller, the DFPW hybrid controller, to be described in Section VIII, is needed.

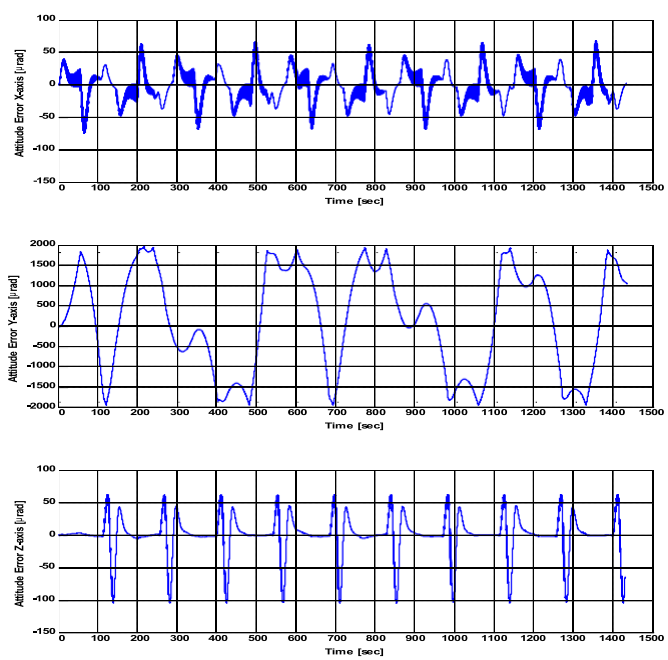


**Fig. 9. Per-axis Attitude Control Errors of the ORS Hybrid Controller**

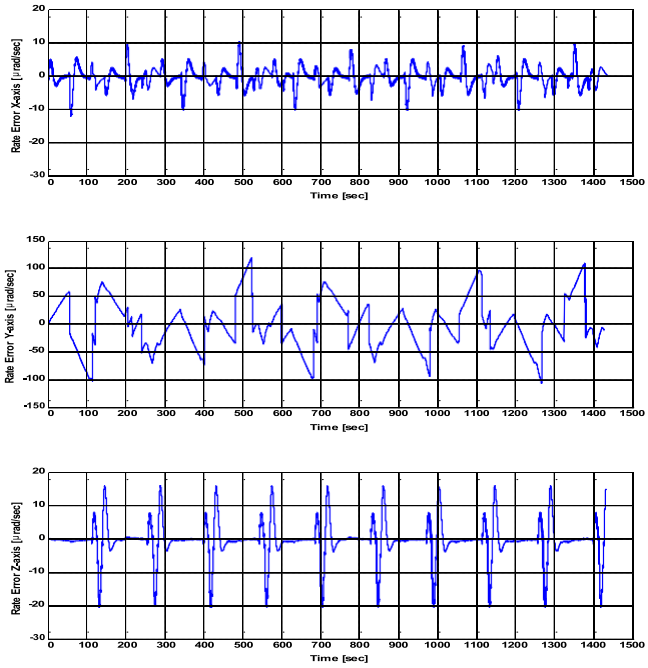


**Fig. 10. Per-axis Attitude Rate Control Errors of the ORS Hybrid Controller**

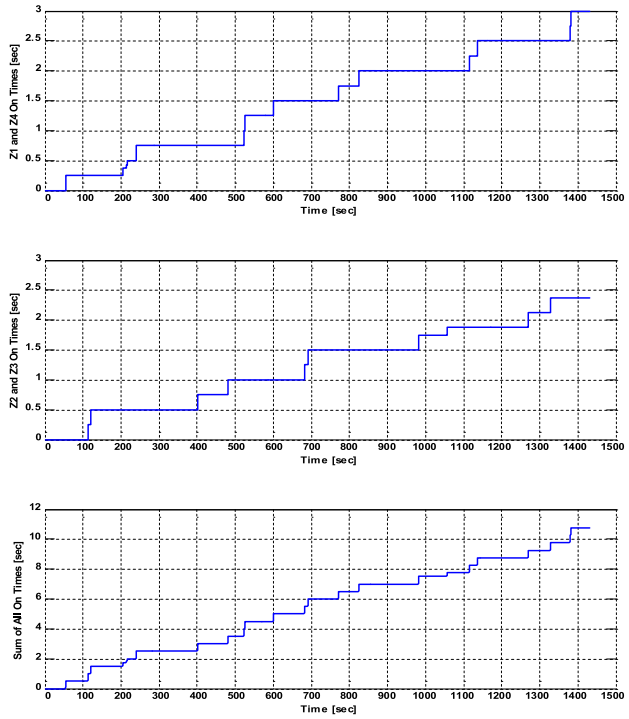


**Fig. 11. Accumulated $Z_i$ (i=1–4) Thrusters' On-time's**

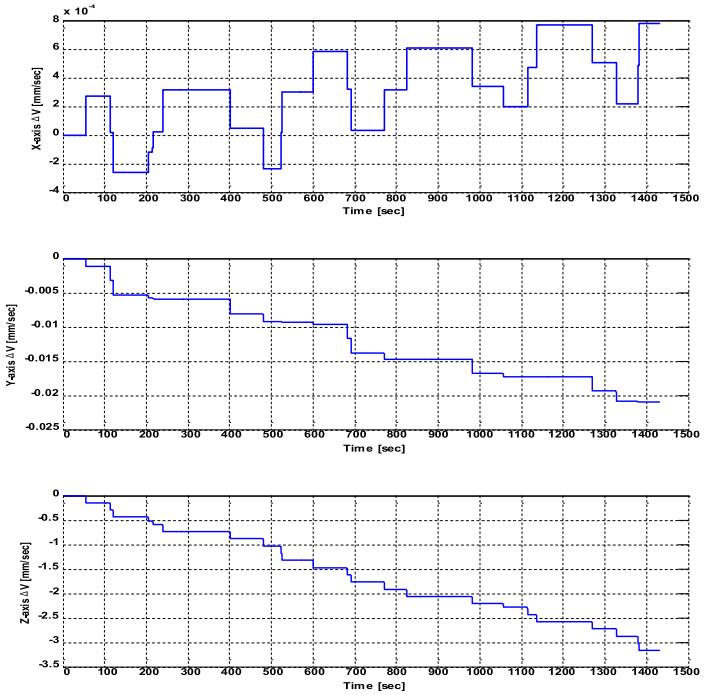


**Fig. 12. Accumulated ΔV Imparted on the Spacecraft**

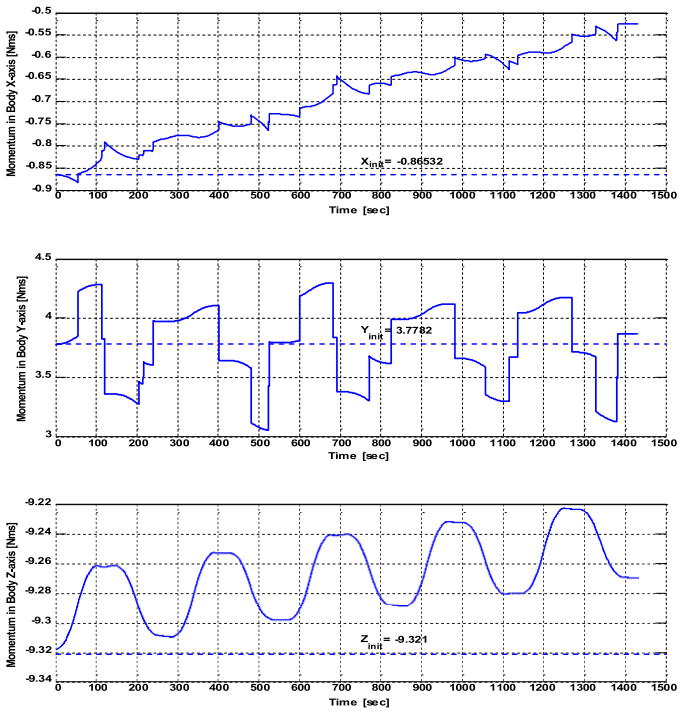


**Fig. 13. Time Histories of the Per-axis Angular Momenta of the Reaction Wheels**

## VIII. Candidate Hybrid Control Architecture for the DFPW Operations Mode

Let us first analyze the couplings between the S/C's X and Z-axis, as well as the Y and Z-axis when RWA-2 and RWA-4 are used to control the S/C's X and Y-axis. As per Section VII, let $-\theta$ be the angle between the S/C's +Y-axis and the projection of the wheel #4 orientation on the X-Y plane of the spacecraft (as measured from the +Y-axis, see also Fig. 3). As per Eq. (1), we have:

$$\begin{bmatrix} T_X \\ T_Y \\ T_Z \end{bmatrix} = \begin{bmatrix} 1/\sqrt{2} & -\sqrt{2/3}\sin\theta \\ 1/\sqrt{6} & +\sqrt{2/3}\cos\theta \\ +1/\sqrt{3} & +1/\sqrt{3} \end{bmatrix} \begin{bmatrix} T_2 \\ T_4 \end{bmatrix}, \tag{6}$$

$$B = \begin{bmatrix} 1/\sqrt{2} & -\sqrt{2/3}\sin\theta \\ 1/\sqrt{6} & \sqrt{2/3}\cos\theta \end{bmatrix} \tag{7}$$

The matrix B is the 2×2 mapping matrix between wheel 2/4 and the spacecraft's X/Y axes. It is formed using the first and second rows of the 3×2 matrix given in Eq. (6). Let $[T_X\ T_Y]^T$ be the [X, Y] torque command vector that is needed by the RWA controller. To generate this torque vector using reaction wheel #2 and #4, one can use the "pseudo inverse" solution of the mapping matrix B:

$$\begin{bmatrix} T_2 \\ T_4 \end{bmatrix} = [B^T B]^{-1} B^T \begin{bmatrix} T_X \\ T_Y \end{bmatrix} \tag{8}$$

If the desired torque is about the X-axis, then, substitution of $[T_X\ T_Y]^T = [1, 0]^T$ into Eq. (8), and then back substitution of the resultant $[T_2\ T_4]^T$ into Eq. (6) give:

$$\begin{bmatrix} T_X \\ T_Y \\ T_Z \end{bmatrix} = \begin{bmatrix} +1 \\ 0 \\ -\frac{1}{9\sqrt{2}}(\sin\theta + \sqrt{3}\cos\theta)(1 + 2\cos\theta)/\Delta \end{bmatrix}$$

$$\Delta = \frac{1}{3} - \frac{2}{9}\sin^2\theta + \frac{1}{3\sqrt{3}}\sin 2\theta \tag{9}$$

Note that, the desired X and Y-axis torque commands are achieved <u>exactly</u> but there is an unwanted coupling torque generated about the Z-axis. Similarly, if the desired torque is about the Z-axis, substitution of $[T_X\ T_Y]^T = [0, 1]^T$ into Eq. (8), and then back substitution of the resultant $[T_2\ T_4]^T$ into Eq. (6) give:

$$\begin{bmatrix} T_X \\ T_Y \\ T_Z \end{bmatrix} = \begin{bmatrix} 0 \\ 1 \\ +\frac{1}{9\sqrt{2}}(\sin\theta + \sqrt{3}\cos\theta)(\sqrt{3} - 2\cos\theta)/\Delta \end{bmatrix} \tag{10}$$

Here, $\delta$ was defined in Eq. (9). Again, there is an unwanted coupling torque generated about the Z-axis. The X/Z and Y/Z coupling terms, given in Eq. (9) and (10), respectively, are depicted in Fig. 14. Note that a positive X-axis torque command will generate a positive Z-axis coupling torque, while a positive Y-axis torque command will generate a negative Z-axis coupling torque. From Eq. (9), we note that $\delta$ becomes zero when $\theta$ = -60˚ or +120˚. At these angles, the numerators of the two $T_Y$ terms in Eqs. (9–10) also become zero. But, in the limit, the coupling coupling terms become *infinity*. With either of these articulation angles, the rank of the matrix "B" in Eq. (7) becomes 1. As such, control of S/C's X and Y could not be performed using RWA-2 and RWA-4 (in this articulated position). These articulation angles are to be avoided.

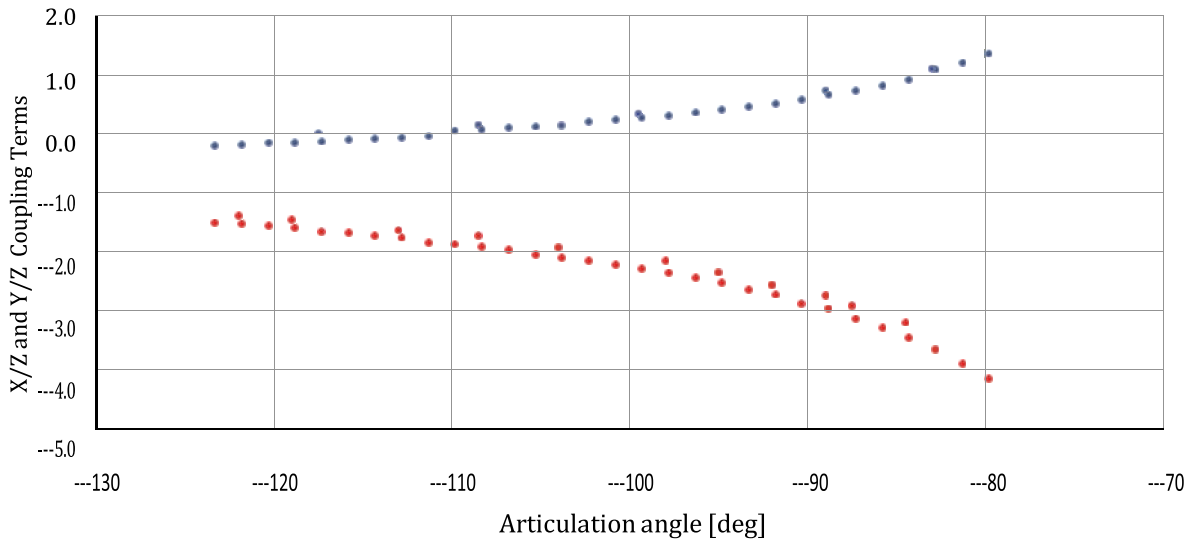


**Fig. 14. Variations of the X/Z and Y/Z Coupling Terms with Articulation Angle (Blue: X/Z coupling, and Red: Y/Z coupling)**

In Section VII, we concluded that to achieve good performance for the ORS hybrid controller, we want $\theta_{optimal}$ = –94.2˚. With this articulation angle, the X/Z and Y/Z coupling terms for the DFPW hybrid controller are +0.537 and -2.344, respectively (see Fig. 14). These coupling terms look large, but in reality, in the DFPW mode, both the S/C's X and Y-axis are only being maintained in a quiescent state (no slew). Past flight experience indicates that the magnitude of these X and Y-axis torque commands are very small. From Fig. 14, we note that smaller coupling terms could be achieved using other articulation angles (e.g., $\theta_{optimal}$ = –120˚). But it will be highly unproductive to make frequent articulation angle changes between the ORS and DFPW operation modes. Hence, the same $\theta_{optimal}$ = –94.2˚ is used for both the ORS and DFPW hybrid controllers.

Nominally, in DFPW operations mode, the S/C is being commanded to spin about the Z-axis. With this spin rate, the six Fields, Particles, and Plasma Waves instruments collect science data as they scan the 360˚ sky. But rotating the S/C (with spinning RWAs) will lead to excessive firings of the Y-facing thrusters, wasting hydrazine. One way to conserve hydrazine when using the DFPW hybrid controller is described below. First, the Y-facing thrusters are fired for a pre-determined duration to impart an initial rate about the S/C's Z-axis spacecraft. Thereafter, without any more thrusters' firing, the S/C's Z-axis rate will fluctuate according to the conservation of the total angular momentum of the spacecraft system in an inertial frame. This oscillation of the Z-axis spin rate should not be a problem for the six Fields, Particles, and Plasma Wave instruments. Scientific data could still be collected and the spacecraft's attitude at which these science data are collected are readily available from the spacecraft telemetry data. At the same time, the two reaction wheels could maintain the stringent pointing control requirement of 3.14 mrads (X and Y-axis, radial 99%), meeting the pointing requirement of the HGA.[1]

Let $I_{ZZ}$ be the Z-axis MOI of the spacecraft, $\Omega_Z(t)$ be the S/C's Z-axis angular rate at time t, and $\Omega_Z(0) = \Omega_0$. The angular momenta of the two controlling wheels, RWA-2 and RWA-4, about the S/C's X, Y, and Z-axis, are denoted by $H_X(t)$, $H_Y(t)$, and $H_Z(t)$, respectively.

$$\begin{bmatrix} \cos\alpha(t) & -\sin\alpha(t) & 0 \\ \sin\alpha(t) & \cos\alpha(t) & 0 \\ 0 & 0 & 1 \end{bmatrix} \begin{bmatrix} H_X(t) \\ H_Y(t) \\ I_{ZZ}\Omega_Z(t)+H_Z(t) \end{bmatrix} = \begin{bmatrix} H_X(0) \\ H_Y(0) \\ I_{ZZ}\Omega_0+H_Z(0) \end{bmatrix} \tag{11}$$

In Eq. (11), the angle $\alpha(t)$ is the angular displacement of the S/C's X-axis at time t relative to the initial position of the S/C's X-axis at time t = 0 (when thrusters' firings have just stopped). This angle is related to the non-uniform spin rate $\Omega_Z(t)$ by:

$$\alpha(t) = \int_{\tau=0}^{\tau=t} \Omega_Z(\tau)\, d\tau \tag{12}$$

From Eq. (6), we note that the per-axis angular momenta $H_X(t)$, $H_Y(t)$, and $H_Z(t)$ are related to the two per-wheel angular momenta $H_2(t)$ and $H_4(t)$, by:

$$
\begin{bmatrix} H_X(t) \\ H_Y(t) \\ H_Z(t) \end{bmatrix} = \begin{bmatrix} 1/\sqrt{2} & -\sqrt{2/3}\sin\theta \\ 1/\sqrt{6} & +\sqrt{2/3}\cos\theta \\ +1/\sqrt{3} & +1/\sqrt{3} \end{bmatrix} \begin{bmatrix} H_2(t) \\ H_4(t) \end{bmatrix} \tag{13}
$$

Here, the articulation angle θ is –94.2°. Using Eqs. (11–13), the time-varying S/C's Z-axis spin rate is given by:

$$
\begin{aligned}
\omega_Z(t) &= \omega_0 + \Delta\omega_Z(t) \\
&= \omega_0 + \frac{1}{I_{ZZ}}[p_X\{H_X(0)(1-\cos\Delta\theta(t))-H_Y(0)\sin\Delta\theta(t)\} + p_Y\{H_Y(0)(1-\cos\Delta\theta(t))+H_X(0)\sin\Delta\theta(t)\}]
\end{aligned} \tag{14}
$$

where:

$$
p_X = -\frac{2\cos\theta+1}{\sqrt{6}\cos\theta+\sqrt{2}\sin\theta} = +0.5369 \ (\text{if } \theta = -94.2^\circ) \qquad p_Y = +\frac{\sqrt{3}-2\sin\theta}{\sqrt{6}\cos\theta+\sqrt{2}\sin\theta} = -2.3442 \ (\text{if } \theta = -94.2^\circ)
$$

Using Eqs. (13–14), analytical expressions for the maximal and minimal values of $\Delta\Omega_Z(t)$ are derived and given in Eq. (15). The parameters $K_1$ and $K_2$ used in Eq. (15) were defined in Appendix C. Both parameters are functions of the initial S/C's X and Y-axis angular momenta $H_X(0)$ and $H_Y(0)$. Contour plots of the maximal and minimal values of $\Delta\Omega_Z(t)$, as functions of $H_X(0)$ and $H_Y(0)$, are given in Figs. 15 and 16, respectively.

$$
\Delta\omega_Z[\max] = +\frac{1}{I_{ZZ}}\{K_1+\sqrt{K_1^2+K_2^2}\} \qquad \Delta\omega_Z[\min] = +\frac{1}{I_{ZZ}}\{K_1-\sqrt{K_1^2+K_2^2}\} \tag{15}
$$

The maximal and minimal values of the reaction wheel rates, $\Omega_2(t)$ and $\Omega_4(t)$, are given in Eq. (16). The parameters $J_i$ (i=1–4) used in Eq. (16) are also defined in Appendix C. These parameters are also functions of $H_X(0)$ and $H_Y(0)$. Contour plots of the maximal and minimal values of $\Omega_2(t)$, in units of rpm, as functions of $H_X(0)$ and $H_Y(0)$ are given in Figs. 17 and 18. Contour plots of maximal and minimal values of $\Omega_4(t)$, in units of rpm, are identical to those of $\Omega_2(t)$. They are not repeated here. The moments of inertia of wheels are identical and are denoted by $I_{RWA}$.

$$
\begin{aligned}
\Omega_2[\max] &= +\frac{\sqrt{J_1^2+J_2^2}}{I_{RWA}}\frac{60}{2\pi}, & \Omega_2[\min] &= -\frac{\sqrt{J_1^2+J_2^2}}{I_{RWA}}\frac{60}{2\pi} \\
\Omega_4[\max] &= +\frac{\sqrt{J_3^2+J_4^2}}{I_{RWA}}\frac{60}{2\pi}, & \Omega_4[\min] &= -\frac{\sqrt{J_3^2+J_4^2}}{I_{RWA}}\frac{60}{2\pi} \\
\sqrt{J_1^2+J_2^2} &= \sqrt{J_3^2+J_4^2}
\end{aligned} \tag{16}
$$

Also given in Appendix C is the time history of the rotation angle α(t) defined in Eq. (12). The parameters $G_1$ and $G_2$ used in Eq. (17) were defined in Appendix C. These parameters are functions of $I_{ZZ}$, $\Omega_0$, and $K_i$ (i=1–2). The period of the Z-axis rotational motion is given in Eq. (18). The average spin rate of the DFPW hybrid controller is given in Eq. (19).

$$
\Delta\theta(t) = 2\tan^{-1}\left\{\frac{\sqrt{G_1^2-G_2^2}}{G_1-G_2}\tan\left(\frac{\sqrt{G_1^2-G_2^2}}{2}t\right)\right\} - \tan^{-1}\frac{K_2}{K_1} \tag{17}
$$

$$
T_{Period} = \frac{2\pi}{\sqrt{G_1^2-G_2^2}}, \qquad G_1^2-G_2^2 > 0 \tag{18}
$$

$$
\omega_{Avg} = \sqrt{\omega_0^2 + \frac{2\omega_0}{I_{ZZ}}\left(K_1 - \frac{K_2^2}{2\omega_0 I_{ZZ}}\right)} \tag{19}
$$

The performance of the DFPW hybrid controller is evaluated using the science observation sequence performed on 2012-054T22:14:00.00. The spacecraft was commanded to spin about the positive Z-axis at a constant rate of 3.07 mrad/s. The total slew angle was 5,040° (14 revolutions). The total spin time of the spacecraft, from rest to rest, was 08:07:49 (or 29,269 s). Values of key parameters of the simulated spacecraft system are identical to those summarized in Table 1. This DFPW scenario will be executed using both the DFPW hybrid controller and the all-thruster controller.

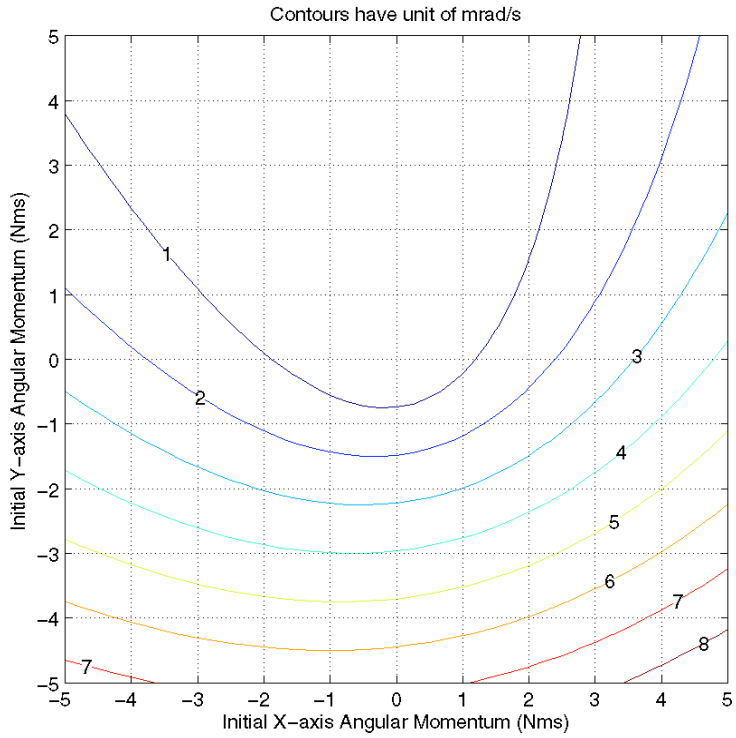


**Fig. 15. Variation of the $\Delta\Omega_Z$ [max] With the Initial X and Y-axis Angular Momenta**

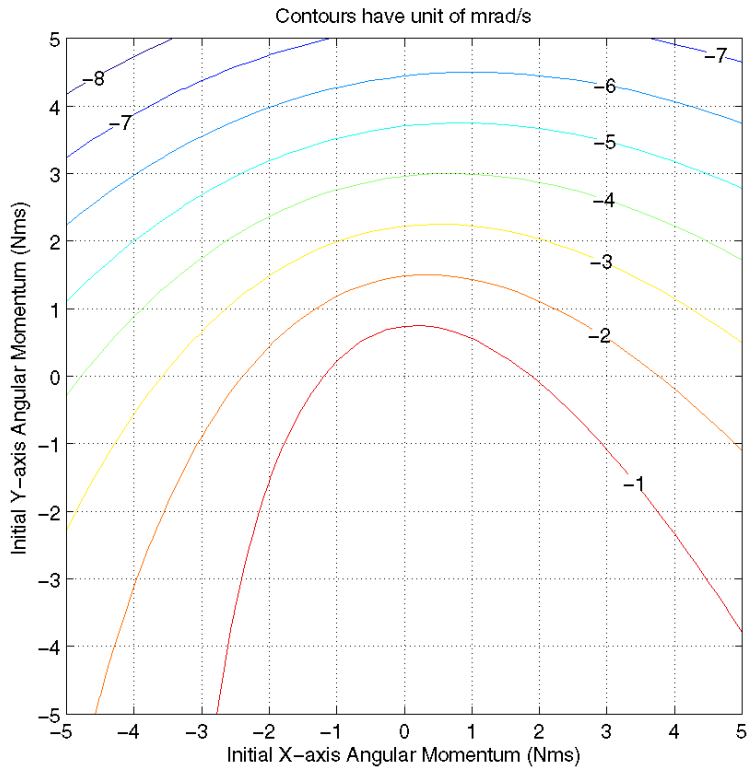


**Fig. 16. Variation of the $\Delta\Omega_Z$ [min] With the Initial X and Y-axis Angular Momenta**

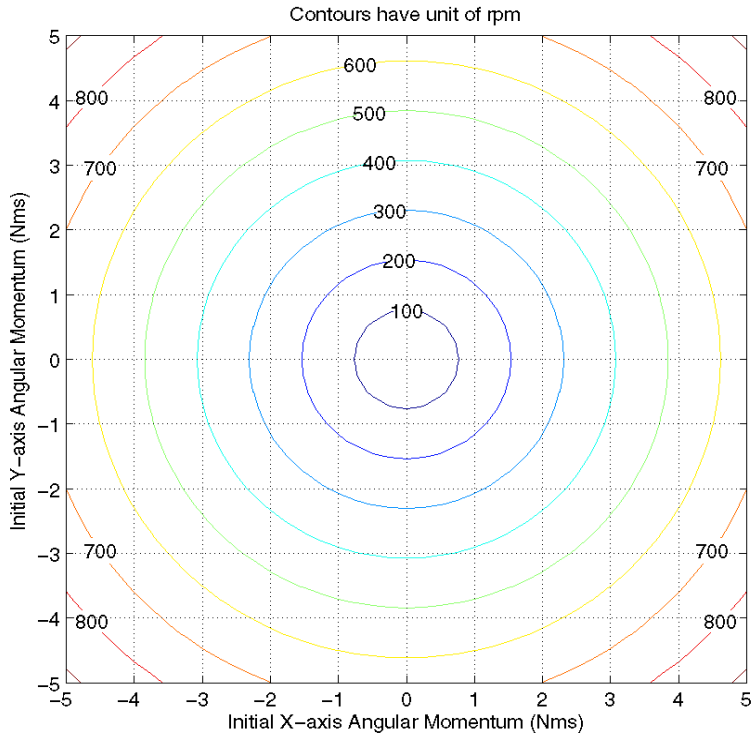


**Fig. 17. Variation of the $\Omega_2$ [max] With the Initial X and Y-axis Angular Momenta**

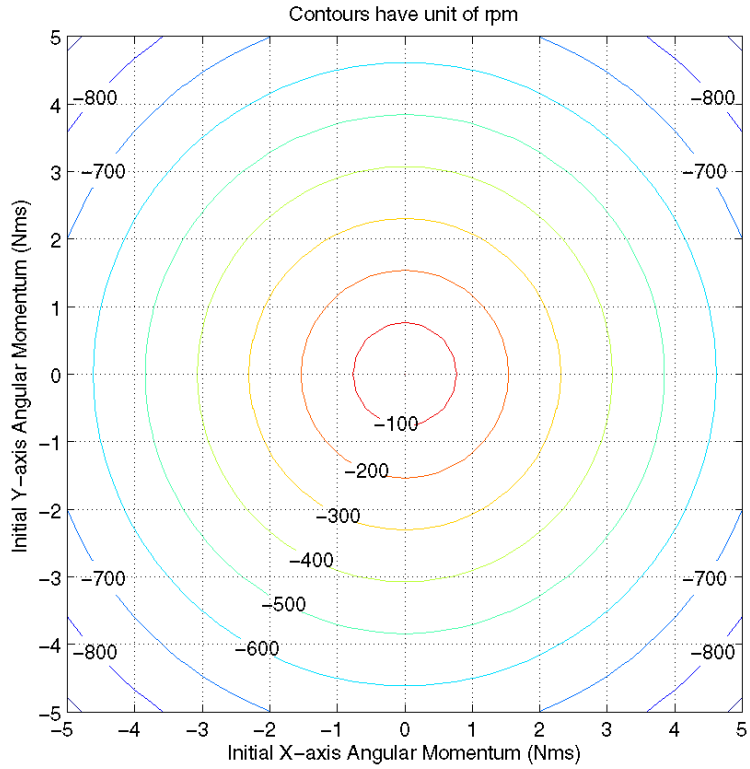


**Fig. 18. Variation of $\Omega_2$ [min] With the Initial X and Y-axis Angular Momenta**

To use the DFPW hybrid controller, one must select appropriate initial angular momenta $H_X(0)$ and $H_Y(0)$ using the contour plots (Figs. 15–18). If we select $H_X(0)=H_Y(0)= -3$ Nms, we have $\Delta\Omega_Z(\max) \approx 4.44$ mrad/s and $\Delta\Omega_Z(\min) \approx -1.36$ mrad/s. Accordingly, the peak S/C's Z-axis rotation rate is 3.07+4.44 = 7.51 mrad/s which is outside the performance limit of the Cassini's star tracker. This problem could be overcome by a "suspension" of the use of the star tracker. During this "tracker suspension" period, the S/C's attitude is propagating using only the gyroscopes. This technique has been practiced on Cassini over the years 2004–2012, as reported in Ref. 1. The lowest S/C's Z-axis rotation rate is 3.07–1.36 = 1.71 mrad/s. This will not cause a reversal of the rotation direction. However, the spin rates of RWA-2 and RWA-4 will fluctuate within ±552 rpm. That is, the bearings will operate inside their EHD limit (about ±300 rpm) a significant percent of the sequence time. This is a disadvantage.

The situation is improved if we pick $H_X(0)=H_Y(0)= -4$ Nms. The resultant $\Delta\Omega_Z(\max) \approx 5.92$ mrad/s and $\Delta\Omega_Z(\min) \approx -1.81$ mrad/s. Accordingly, the peak S/C's Z-axis rotation rate is 3.07+5.92 = 8.99 mrad/s. The performance of the DFPW hybrid controller is given in Figs. 19–21. Note that only the time histories of various system variables in the first 4,000 s of the 29,269-s DFPW spinning scenario are given in these figures. The per-axis spacecraft's rates achieved by the DFPW hybrid controller are depicted in Fig. 19. Note that, the DFPW hybrid controller achieved quiescent rates about both the S/C's X and Y-axis. On the other hand, the Z-axis rate fluctuated with time. The maximum and minimum Z-axis rates agree closely with the predicted values. The period of the Z-axis spin rate, given in Fig. 19, is 1,867 s. This closely matched that predicted using Eq. (18) (which is 1,868 s). As depicted in Fig. 20, the spin rates of the two controlling reaction wheels fluctuated about the 0-rpm. The peak rate of these wheels (±729 rpm) closely matched that predicted (±736 rpm). Approximately, these wheels spent 19% of time inside the EHD rate limit of the ball bearings.[#] The X and Y-axis attitude control errors are given in Fig. 21. Since the selected angular momenta $H_X(0)=H_Y(0) = -4$ Nms fall underneath the boundary depicted in Fig. 22, the average S/C's rate $\Omega_{Avg} > \Omega_0$ (See also Eqn. (19)). That is, in a given time span, the Z-axis displacement covered by the DFPW hybrid controller is larger than that of the nominal controller, which is an advantage. The performance of the all-thruster controller for this DFPW scenario is documented in Appendix B. A comparison of the key figures of merit of these two controllers is given in Table 3.

**Table 3. Figures of Merit: DFPW Hybrid Controller vs. All-thruster Controller**

| Figures of Merit | Units | DFPW Hybrid Controller | All-thruster Controller[a] |
|---|---|---|---|
| Peak Attitude Control Error: | | | |
| X-xis | mrads | ±0.01 | ±2.0 |
| Y-xis | mrads | ±0.01 | ±2.0 |
| Peak Instantaneous Rate: | | | |
| X-xis | mrad/s | ±0.0015 | ±0.05 |
| Y-xis | mrad/s | ±0.0015 | ±0.05 |
| Z- | xis spin rate | mrad/s | 3.07+ΔΩ[b] |
| 3.07±0.05 Time to complete 10 rev. | | Hour | |
| 5.1861 | 5.6851 | | |
| Total Hydrazine Consumption | gram | 9.92[c] | 34.2 |
| Total ΔV magnitude imparted at S/C | mm/s | 0[d] | 20.63 |

[a]With per-axis attitude control dead-band of [2,2,20] mrads. See Appendix B for details.
[b]$\Delta\Omega[\max] = +5.92$ mrad/s, and $\Delta\Omega[\min] = -1.81$ mrad/s.
[c]Spin-up and spin-down of S/C to/from 3.07 mrad/s ≈ 3.07e-3×3518×2/1.234/(180×9.806) ≈ 9.92 grams.
[d]Spin-up and spin-down are performed via thruster couples. Net ΔV imparted on the S/C is nearly zero.

[#] One way to lower the percent time the bearings spent inside the EHD limits is to start the Z-axis rotation with "larger" $H_X(0)$ and $H_Y(0)$. For example, if we use $H_X(0) = -4$ Nms and $H_Y(0) = -5$ Nms, the resultant RWA-2/4 spin rates will fluctuate inside ±826 rpm (instead of ±736 rpm). The resultant $\Omega_Z(\max)$ is 10.2 mrad/s (instead of 8.99 mrad/s) and $\Omega_Z(\min) = 1.41$ mrad/s (instead of 1.26 mrad/s). The time the wheel bearings spent inside ±300 rpm will be 15% (instead of 19%). Other "larger" [$H_X(0)$, $H_Y(0)$] combinations will lower the percent time the wheels spent inside the EHD limits even further.

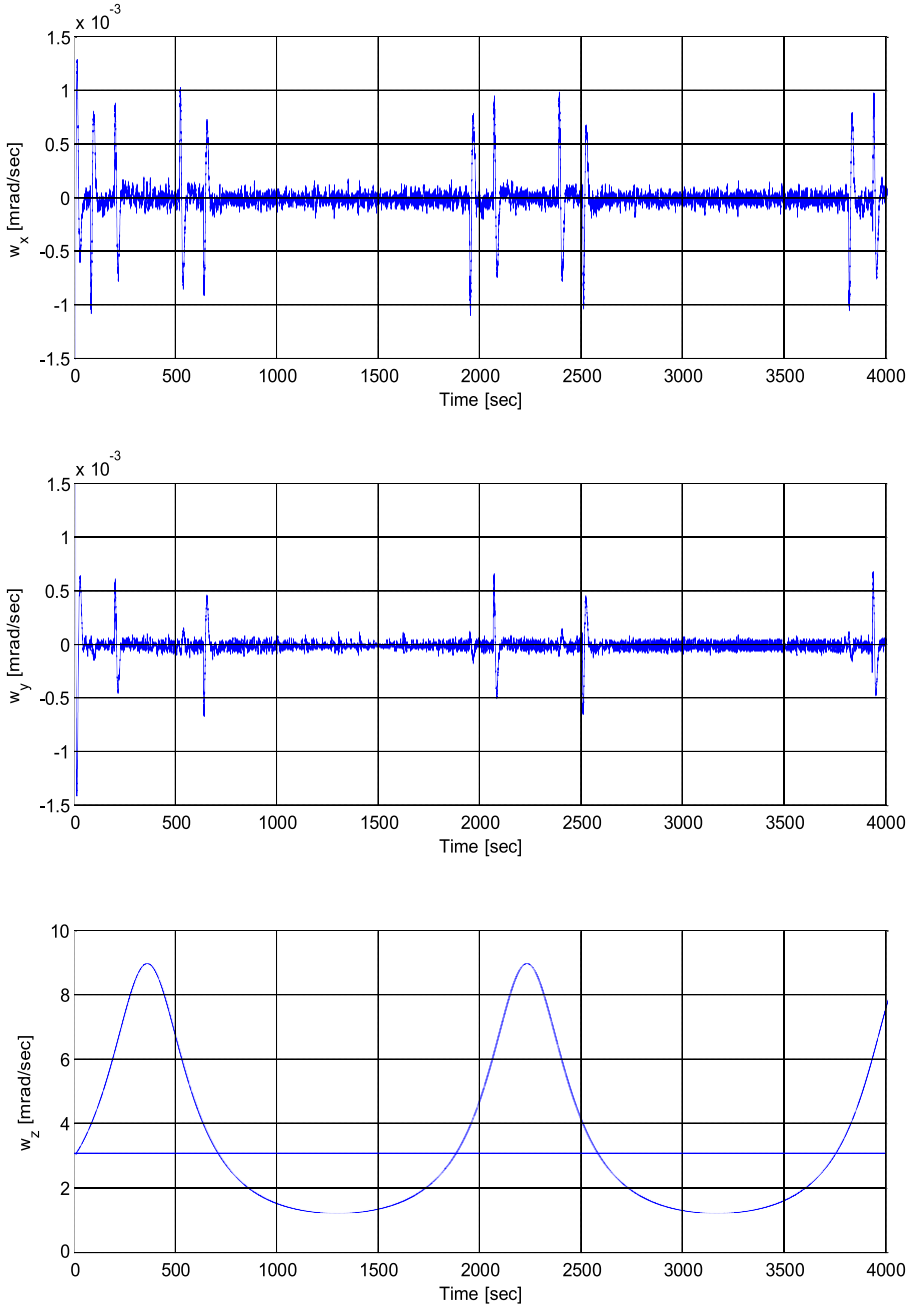


**Fig. 19. Time Histories of the Per-axis S/C's Rates Achieved by the DFPW Hybrid Controller**

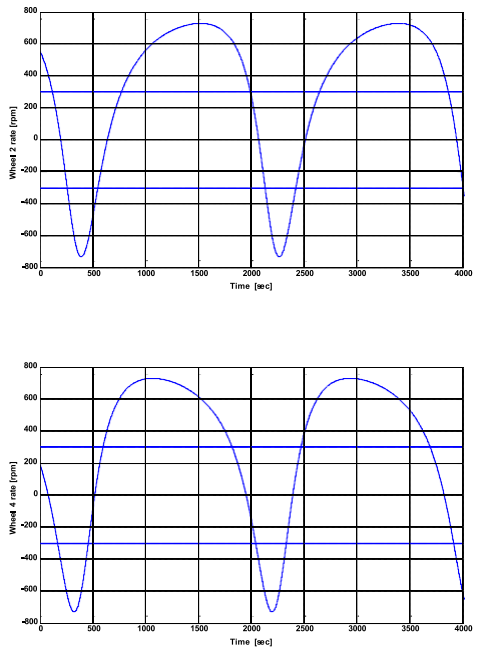


**Fig. 20. Time Histories of the Controlling Wheels' Spin Rates Achieved by the DFPW Hybrid Controller (Two horizontal dashed lines are drawn at ±300 rpm)**

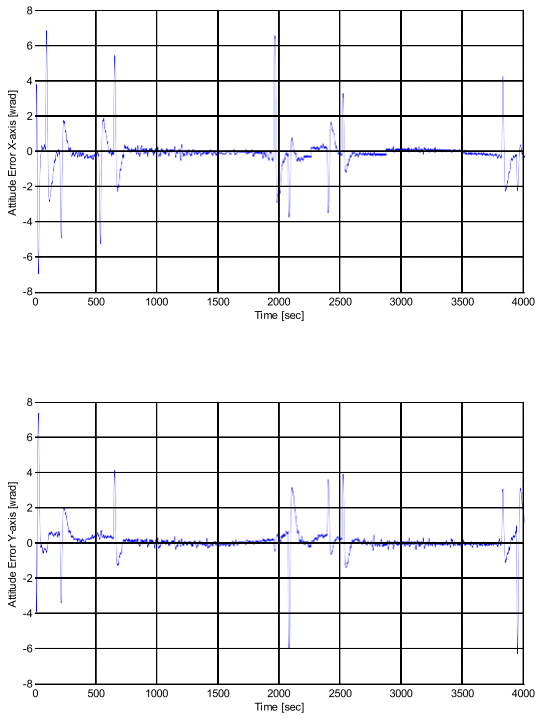


**Fig. 21. Time Histories of the Per-axis Attitude Control Errors Achieved by the DFPW Hybrid Controller**

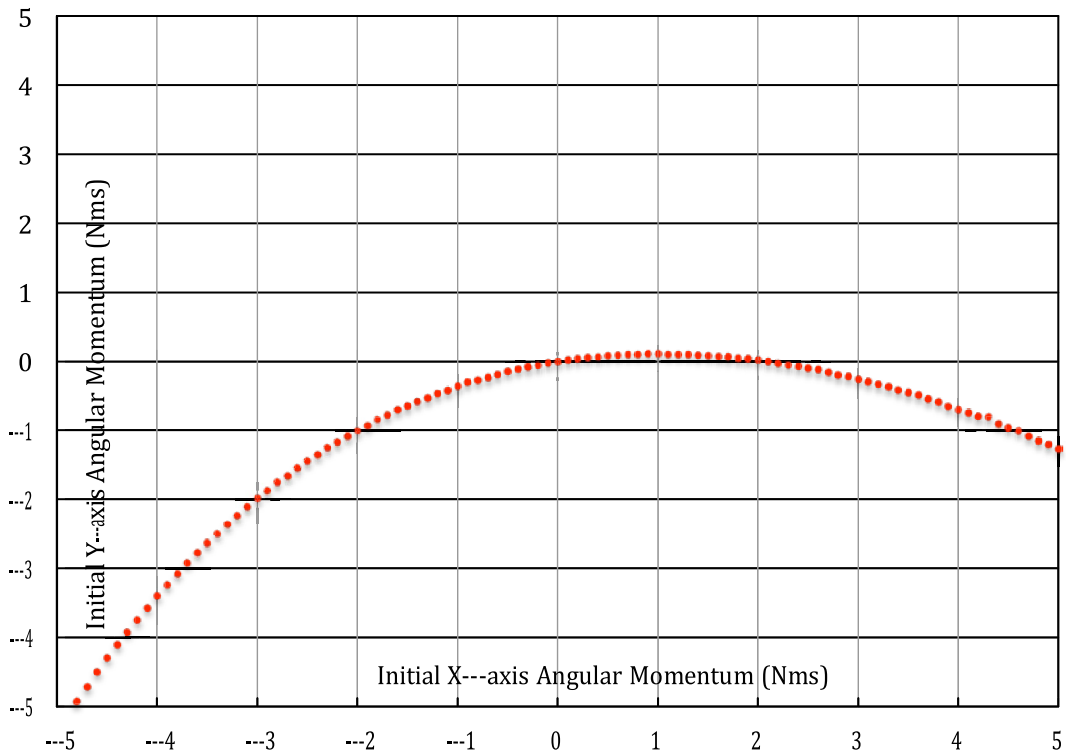


**Fig. 22 All Combinations of Selected [$H_X(0)$, $H_Y(0)$] That Fall Underneath the Boundary Will Have $\Omega_{Avg} \geq \Omega_0$ (See also Eqn. (19))**

## IX. Summary and Conclusions

In this study, we evaluate the feasibility of controlling Cassini using two reaction wheels and a set of four thrusters in meeting the stringent pointing control and stability requirements of two key Cassini science operations modes: the Optical Remote Sensing and Downlink, Fields, Particles, & Waves operation modes. Since RWA-4 is articulable, it should be articulated to a position that minimized the crossing couplings between the X/Y and Z/Y spacecraft acceleration commands. For a representative ORS mosaic scenario, the performance of the ORS hybrid controller is good: Both the attitude and attitude rate control errors are an order of magnitude better than their counterparts achieved using an all-thruster control system. Also, the hydrazine consumption rate of the hybrid controller is about 3.5 times smaller than that of an all-thruster control system. However, large angle rotations about either the X or Z-axis made using this ORS hybrid controller might saturate the reaction wheels. Hence, in DFPW scenarios, a new hybrid controller is needed.

The DFPW hybrid controller could achieve excellent attitude control of the S/C's X and Y-axis, meeting the stringent pointing control requirement of the HGA. But, any attempt to control the S/C's Z-axis spin rate using the Y-facing thrusters will incur heavy hydrazine cost penalty. To work around it, the S/C was first "spun-up" using the Y-facing thrusters to the nominal S/C's Z-axis rate. Thereafter, control about the S/C's Z-axis is "removed", and the spacecraft's Z-axis rate is allowed to fluctuate freely according to the conservation of the total angular momentum of the S/C (in an inertial frame). The resultant peak S/C's Z-axis rate might exceed the functional capability of the Cassini's star tracker. But this could be easily overcome using the flight-proven gyro-based attitude propagation scheme. But one drawback of this "No Z-axis control" scheme is that the spin rates of both reaction wheels will fluctuate about zero-rpm, leading to multiple speed reversals (zero-crossing's) of the wheels' bearings. At the same time, the wheels' rpm will dwell within the EHD speed limits (±300 rpm) for a significant (≈ 19%) time duration. Both conditions are known to cause accelerated degradation of the wheel bearings.

The Cassini flight software would need substantial logic changes to allow the two wheels to be used for attitude control about X and Z-axis during ORS mode and X and Y-axis during DFPW mode. Other supporting software modules such as fault protection, commands and telemetry, etc. must also be modified. The revised flight software

must then be regression tested. The significant effort involved in this endeavor underlines the importance of protecting the health of the reaction wheels.


## Acknowledgments

The work described in this paper was carried out by the Jet Propulsion Laboratory (JPL), California Institute of Technology, under contract with the National Aeronautics and Space Administration. We are indebt to Marcia E. Segura, CIRS team leader at NASA Goddard Space Flight Center, and our JPL colleagues, David Bates, Tom Burk, Laura Burke, Cliff Lee, and Julie L. Webster, for helpful discussions.


## References


[1]Lee, A.Y. and Hanover, G., "Cassini Spacecraft Attitude Control Flight Performance," Paper AIAA-2005-6269, Proceedings of the AIAA Guidance, Navigation, and Control Conference, San Francisco, California, August 15–18, 2005.

[2]Bates, D.M., "Cassini Spacecraft Inflight Swap To Backup Attitude Control Thrusters," Paper AIAA 2010-7559, Proceedings of the AIAA Guidance, Navigation, and Control Conference, August 2–5, 2010, Toronto, Ontario, Canada.

[3]Macala, G.A., "Design of the Reaction Wheel Attitude Control System for the Cassini Spacecraft," Paper AAS 02-121, AAS/AIAA Space Flight Mechanics Meeting, San Antonio, Texas, January 27–30, 2002.

[4]Lee, C. and Lee, A.Y., "Cassini Reaction Wheel Momentum Bias Optimization Tool," Paper AIAA-2005-6271, Proceedings of the AIAA Guidance, Navigation, and Control Conference, San Francisco, California, August 15–18, 2005.

[5]Jaffe, L. and Herrell, L., "Cassini Huygens Science Instruments, Spacecraft, and Mission," Journal of Spacecraft and Rockets, Vol. 34, No. 4, 1997, pp. 509–521.

[6]Pilinski E., and Lee, A.Y., "Pointing Stability Performance of the Cassini Spacecraft," Journal of Spacecraft and Rockets, Volume 46, No. 5, September-October, 2009, pp. 1007–1015.

[7]Tungseth, A.E., "DSP Wheel Recent Experience," Proceedings of the 17th Annual AAS Rocky Mountain Guidance and Control Conference, Keystone, Colorado, February 2–6, 1994, pp. 593–606.

[8]Brown, J., Lam, D., Burk, T., and Wette, M., "The Role of the Flight Software Development System Simulator Throughout the Cassini Mission," Paper AIAA-2005-6389, Proceedings of the AIAA Guidance, Navigation, and Control Conference, San Francisco, California, August 15–18, 2005.

[9]Howett, C. J. A., J. R. Spencer, J. Pearl, and M. Segura (2011), "High Heat Flow From Enceladus' South Polar Region Measured Using 10–600 $cm^{-1}$ Cassini/CIRS Data," Journal of Geophysical Research, 116, E03003, doi:10.1029/2010JE003718.

## Appendix A
## Performance of The All-thruster Controller in An ORS Scenario
## (With [2,2,2] mrad per-axis controller dead-band)

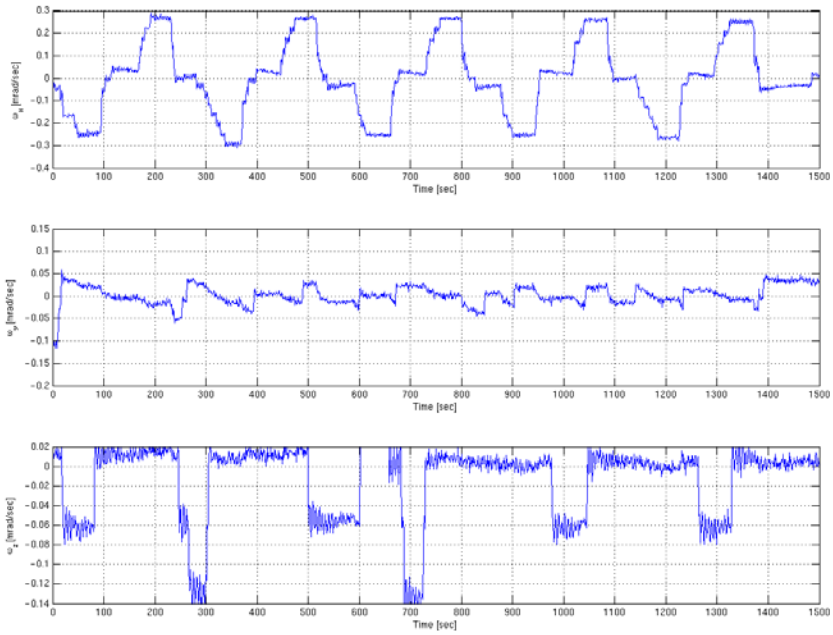


**Fig. A1. Time Histories of Per-axis S/C's Rates**

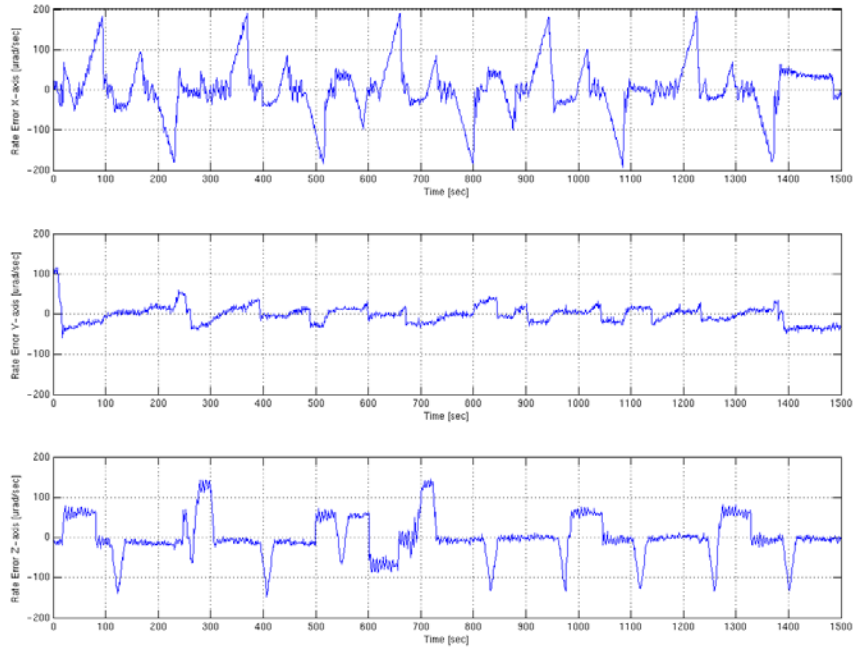


**Fig. A2. Time Histories of Per-axis S/C's Rate Control Errors**

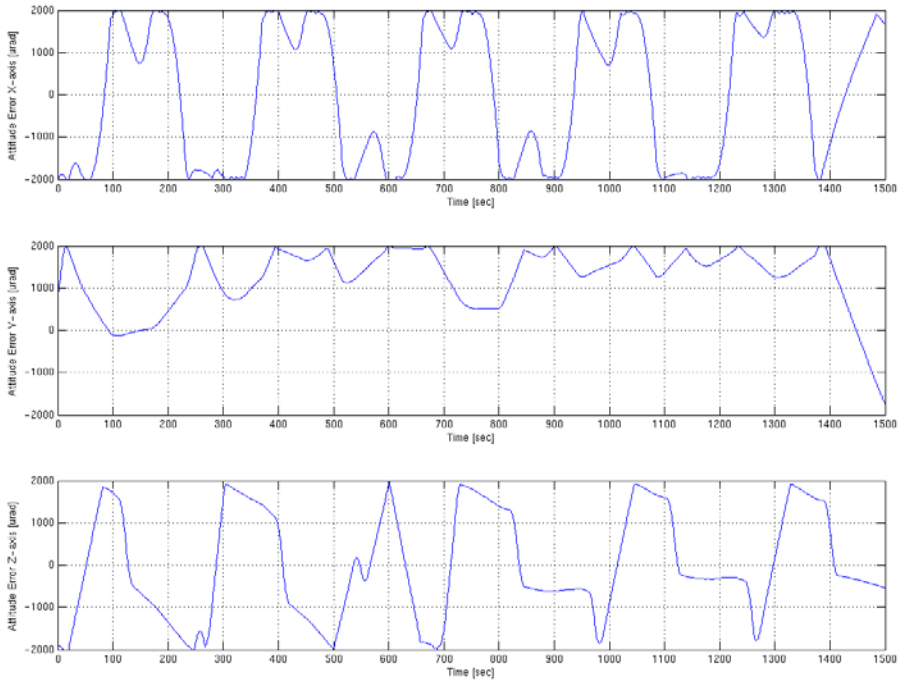


**Fig. A3. Time Histories of Per-axis S/C Attitude Control Errors**

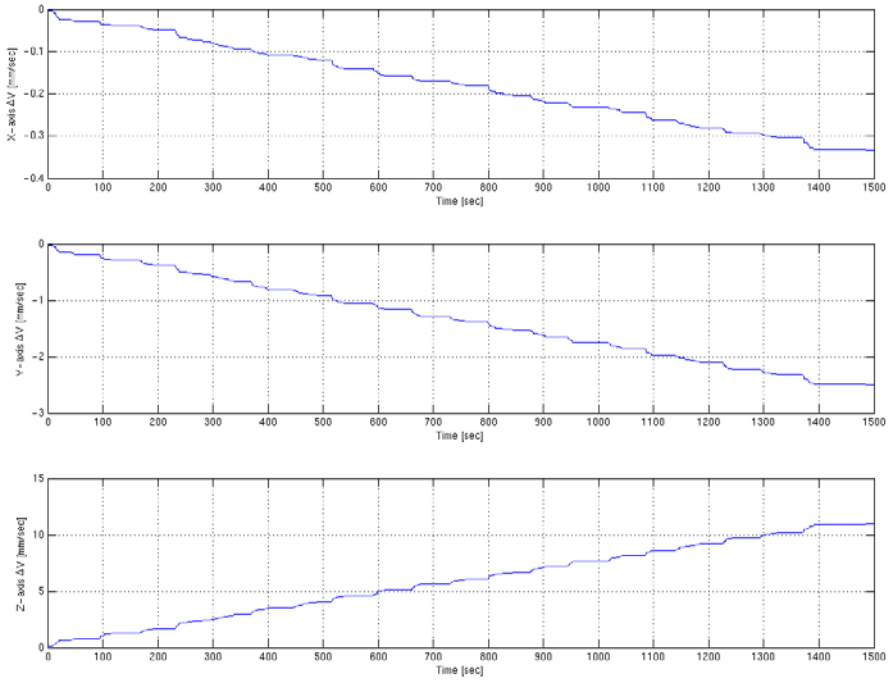


**Fig. A4. Time Histories of ΔV Imparted on the Spacecraft (As Expressed In A J2000 Inertial Coordinate Frame)**

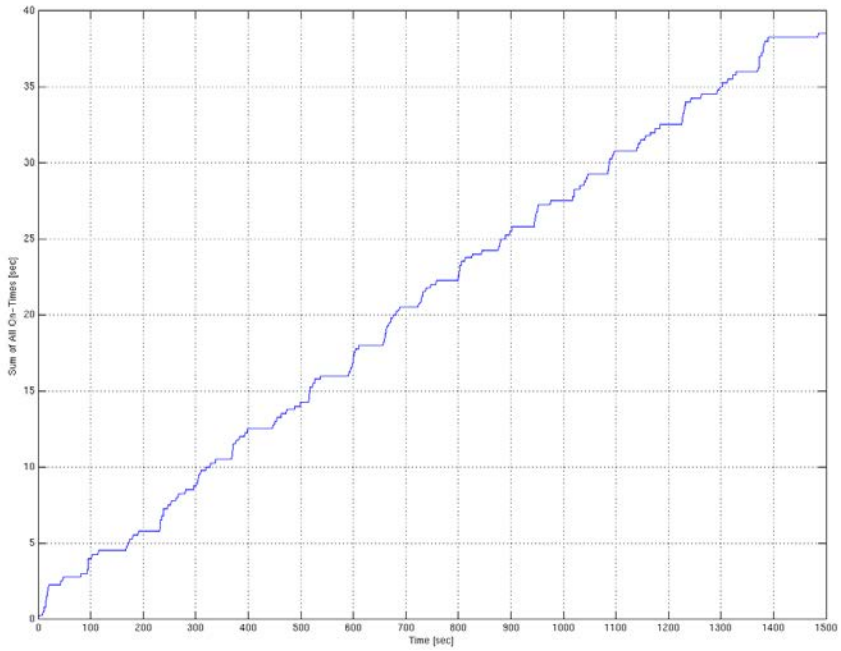


**Fig. A5. Time Histories of the Total Thrusters' On-times**

## Appendix B
## Performance Of The All-thruster Controller In A DFPW Scenario
## (With [2,2,20] mrad per-axis controller dead-band)

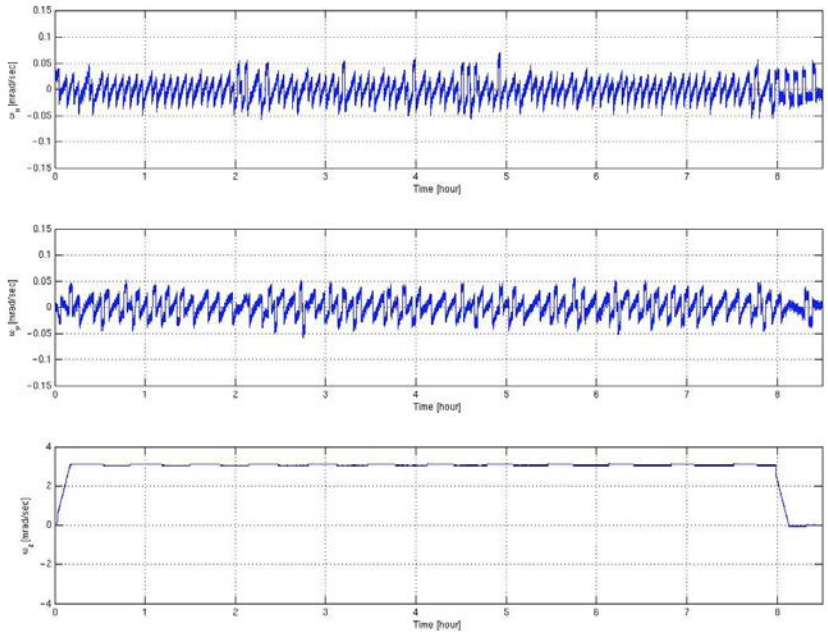


**Fig. B1. Time Histories of Per-axis S/C Rates**

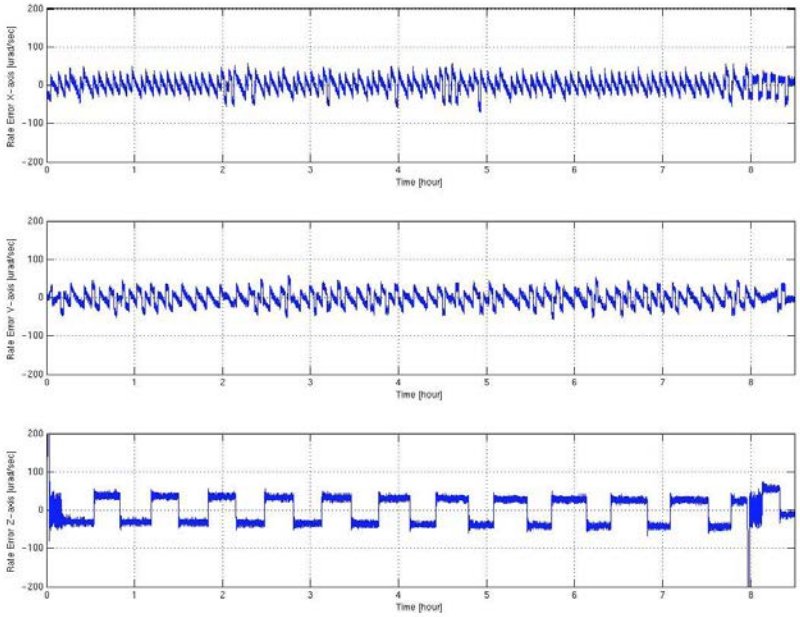


**Fig. B2. Time Histories of Per-axis S/C Rate Control Errors**

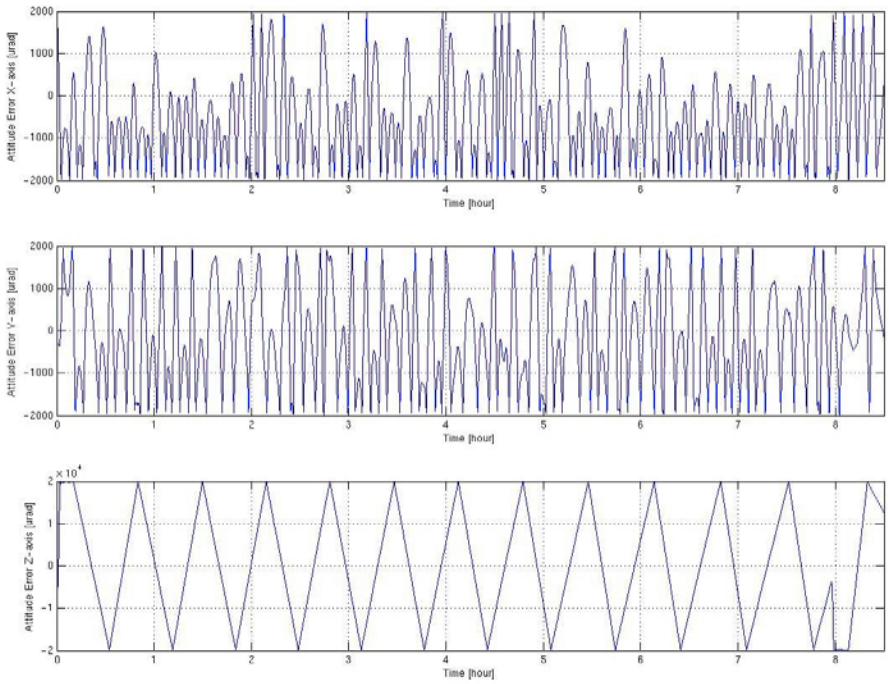


**Fig. B3. Time Histories of Per-axis S/C Attitude Control Errors**

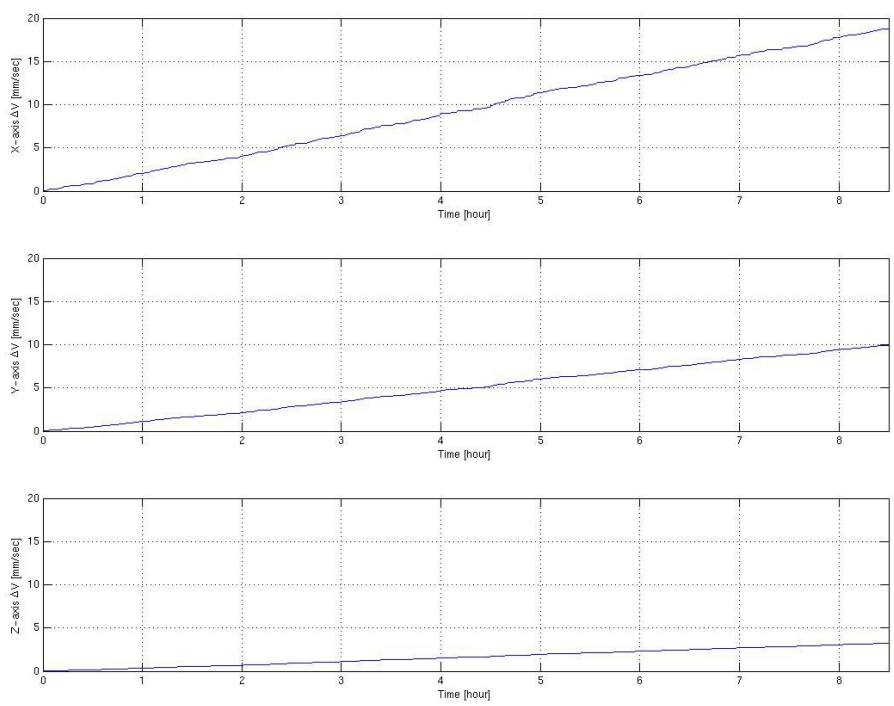


**Fig. B4. Time Histories of ΔV Imparted on the Spacecraft (As Expressed In A J2000 Inertial Coordinate Frame)**

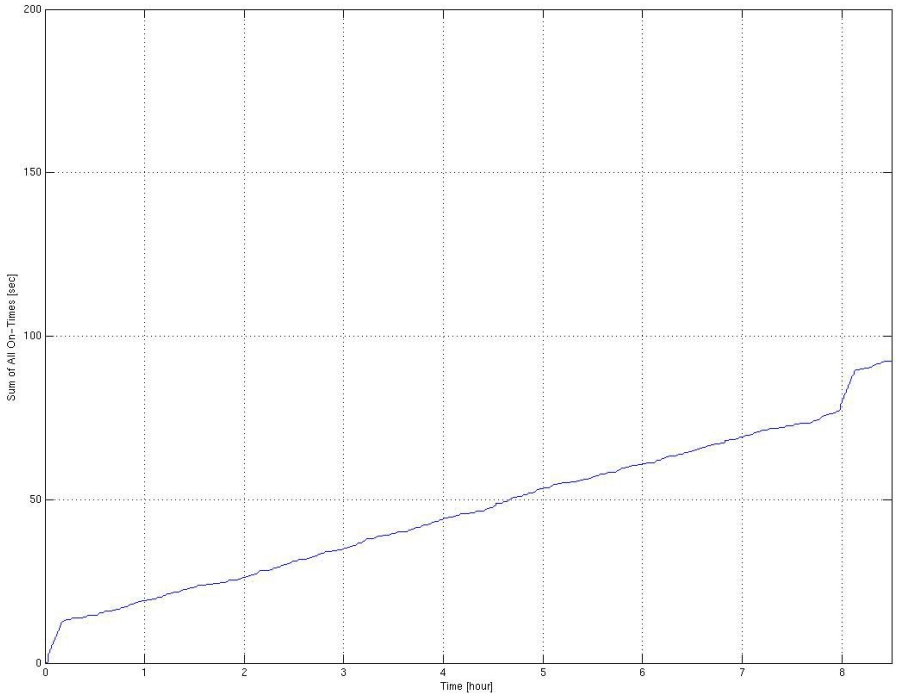


**Fig. B5. Time Histories of the Total Thrusters' On-times**

## Appendix C
## Maximal and Minimal Values of Spacecraft's Z-axis Rate and Reaction Wheels' Spin Rates When Z-axis of the DFPW Hybrid Controller is Uncontrolled

The maximal and minimal values of the S/C's Z-axis rate fluctuation could be determined as follow. From Eq. (14), we have the following expression for the time-varying S/C's Z-axis rate fluctuation $\Delta\Omega_Z(t)$:

$$\Delta\Omega_Z(t) = +\frac{1}{I_{ZZ}}[p_X\{H_X(0)(1-\cos\alpha(t))-H_Y(0)\sin\alpha(t)\} + p_Y\{H_Y(0)(1-\cos\alpha(t))+H_X(0)\sin\alpha(t)\}] \tag{C1}$$

where $p_X$ and $p_Y$ were defined in Eq. (14), and $\alpha(t)$ was defined in Eq. (12). Given the initial values of the X and Y-axis angular momenta of the two RWAs ($H_X(0)$, and $H_Y(0)$), we can define the following parameters:

$$\begin{aligned} K_1 &= +p_X H_X(0) + p_Y H_Y(0) \\ K_2 &= -p_X H_Y(0) + p_Y H_X(0) \end{aligned} \tag{C2}$$

Using these parameters, $\Delta\Omega_Z(t)$ could be rewritten as:

$$\begin{aligned} \Delta\Omega_Z(t) &= +\frac{1}{I_{ZZ}}[K_1\ (1-\cos\alpha(t)) + K_2\sin\alpha(t)] \\ &= +\frac{1}{I_{ZZ}}[K_1\{2\sin^2\frac{\alpha(t)}{2}\} + K_2\{2\sin\frac{\alpha(t)}{2}\cos\frac{\alpha(t)}{2}\}] \\ &= +\frac{2}{I_{ZZ}}\sin\frac{\alpha(t)}{2}[K_1\sin\frac{\alpha(t)}{2} + K_2\cos\frac{\alpha(t)}{2}] \\ &= +\frac{2}{I_{ZZ}}\sqrt{K_1^2+K_2^2}\sin\frac{\alpha(t)}{2}\sin\{\frac{\alpha(t)}{2}+\varepsilon\} \end{aligned} \tag{C3}$$

where: $\varepsilon = \tan^{-1}\{\frac{K_2}{K_1}\}$

The maximal and minimal values of the term $\sin\{\alpha(t)/2\}\sin\{\alpha(t)/2+\varepsilon\}$ are $+\cos^2\{\varepsilon/2\}$ and $-\sin^2\{\varepsilon/2\}$, respectively. Accordingly, the maximal and minimal values of $\Delta\Omega_Z(t)$ are given by the following expressions.

$$\Delta\Omega_Z[\max] = +\frac{1}{I_{ZZ}}\{K_1+\sqrt{K_1^2+K_2^2}\} \qquad \Delta\Omega_Z[\min] = +\frac{1}{I_{ZZ}}\{K_1-\sqrt{K_1^2+K_2^2}\} \tag{C4}$$

Using Eqs. (C1), (C3), and (12) (in Section VIII), one can derive:

$$\begin{aligned} \Omega_Z(t) = \Omega_Z(t) &= \Omega_o + \frac{2}{I_{ZZ}}\sqrt{K_1^2+K_2^2}\sin\frac{\alpha(t)}{2}\sin\{\frac{\alpha(t)}{2}+\varepsilon\} \\ &= \Omega_o + \frac{1}{I_{ZZ}}\sqrt{K_1^2+K_2^2}[\cos\varepsilon - \cos\{\alpha(t)+\varepsilon\}] \\ &= G_1 + G_2\cos\{\alpha(t)+\varepsilon\} \end{aligned} \tag{C5}$$

where:

$$G_1 = \Omega_o + \frac{K_1}{I_{ZZ}}, \qquad G_2 = -\frac{\sqrt{K_1^2+K_2^2}}{I_{ZZ}}$$

From Eq. (C5), we have:

$$\begin{aligned} &\int\frac{d\alpha}{G_1+G_2\cos\{\alpha(t)+\varepsilon\}} = \int dt \\ &\text{Assuming } G_1^2-G_2^2>0 \\ &\alpha(t) = 2\tan^{-1}\{\frac{\sqrt{G_1^2-G_2^2}}{G_1-G_2}\tan\frac{\sqrt{G_1^2-G_2^2}}{2}t\} - \tan^{-1}\frac{K_2}{K_1} \end{aligned} \tag{C6}$$

The maximal and minimal values of the RWA's spin rate could be determined as follow. Using Eqs. (11) and (13) given in Section VIII, we have:

$$
\begin{bmatrix} H_2(t) \\ H_4(t) \end{bmatrix} = \frac{1}{\bullet}\begin{bmatrix} \sqrt{\frac{2}{3}}\cos! & \sqrt{\frac{2}{3}}\sin! \\ \frac{1}{\sqrt{6}} & \left(\frac{1}{\sqrt{2}}\right) \end{bmatrix}\begin{bmatrix} \cos"(t) & \sin"(t) \\ (\sin"(t) & \cos"(t) \end{bmatrix}\begin{bmatrix} H_X(0) \\ H_Y(0) \end{bmatrix} = \begin{bmatrix} J_1\sin"(t) + J_2\cos"(t) \\ J_3\sin"(t) + J_4\cos"(t) \end{bmatrix}
$$

where:

$$
J_1 = \frac{1}{\bullet}\sqrt{\frac{2}{3}}\{\cos! H_Y(0) ( \sin! H_X(0)\} \tag{C7}
$$

$$
J_2 = \frac{1}{\bullet}\sqrt{\frac{2}{3}}\{\cos! H_X(0) + \sin! H_Y(0)\}
$$

$$
J_3 = \frac{1}{\bullet}\frac{1}{\sqrt{2}}\{\frac{1}{\sqrt{3}}H_Y(0) + H_X(0)\}
$$

$$
J_4 = \frac{1}{\bullet}\frac{1}{\sqrt{2}}\{\frac{1}{\sqrt{3}}H_X(0) - H_Y(0)\}
$$

$$
\bullet = (\{\frac{1}{\sqrt{3}}\cos! + \frac{1}{3}\sin!\}
$$

Eq. (C7) could be re-written as follows:

$$
H_2(t) = \sqrt{J_1^2 + J_2^2}\,\sin\{!(t) + "_1\}, \qquad H_4(t) = \sqrt{J_3^2 + J_4^2}\,\sin\{!(t) + "_2\} \tag{C8}
$$

where:

$$
"_1 = \tan^{!1}\{\frac{J_2}{J_1}\} \qquad "_2 = \tan^{!1}\{\frac{J_4}{J_3}\}
$$

From Eq. (C8), we see that the fluctuating angular momenta of RWA-2 and RWA-4 are centered about the 0-rpm spin-rate. The maximal and minimal values of $H_2(t)$ occur when $\alpha$ is $\pi/2-\epsilon_1$ and $-\pi/2-\epsilon_1$, respectively. The corresponding maximal and minimal values of $H_2(t)$ are given in Eq. (C9). The maximal and minimal value of $H_4(t)$ are identical to their $H_2(t)$ counterparts.

$$
H_2[\max] = +\sqrt{J_1^2 + J_2^2}, \qquad H_2[\min] = -\sqrt{J_1^2 + J_2^2}
$$

$$
H_4[\max] = +\sqrt{J_3^2 + J_4^2}, \qquad H_4[\min] = -\sqrt{J_3^2 + J_4^2} \tag{C9}
$$

Note that: $\sqrt{J_1^2 + J_2^2} = \sqrt{J_3^2 + J_4^2}$

## Appendix D
## Special Case with Articulation Angle $\theta = -120^\circ$

In the special case when the articulation angle selected ($\theta$) is $-120^\circ$, the reaction wheel RWA-4 is aligned with RWA-3. The following relations could be derived using the general equations given in the main text and Appendix C. Symbols used here were defined in either the main text or Appendix C. From Eq. (14), we have:

$$p_X = 0, \qquad p_Y = -\sqrt{2}. \tag{D1}$$

From Eqs. (C2) and (C3), we have:

$$K_1 = -\sqrt{2}H_Y(0), \qquad K_2 = -\sqrt{2}H_X(0).$$

$$\Omega_Z(t) = \frac{2\sqrt{2}}{I_{ZZ}}\sqrt{H_X^2(0) + H_Y^2(0)}\,\sin\frac{\Omega(t)}{2}\,\sin\left\{\frac{\Omega(t)}{2} + \tan^{-1}\frac{H_X(0)}{H_Y(0)}\right\} \tag{D2}$$

Based on Eq. (15), the maximal and minimal values of the spacecraft's Z-axis rate $\Omega_Z(t)$ are given by:

$$\Omega_Z(\max) = \Omega_0 + \frac{\sqrt{2}}{I_{ZZ}}\left\{-H_Y(0) + \sqrt{2}\sqrt{H_X^2(0) + H_Y^2(0)}\right\} \tag{D3}$$

$$\Omega_Z(\min) = \Omega_0 + \frac{\sqrt{2}}{I_{ZZ}}\left\{-H_Y(0) - \sqrt{2}\sqrt{H_X^2(0) + H_Y^2(0)}\right\}$$

Based on Eq. (19), the average Z-axis rate of the spacecraft is given by the following expression.

$$\Omega_{AVG} = \sqrt{\Omega_0^2 - \frac{2\sqrt{2}\Omega_0}{I_{ZZ}}H_Y(0) - 2\left(\frac{H_X(0)}{I_{ZZ}}\right)^2} \tag{D4}$$

Based on Eq. (16), the peak spin rates of the two reaction wheels, RWA-2 and RWA-4, are identical, and are given by the following expressions.

$$\Omega_{RWA2}(\max) = \frac{\sqrt{2}}{I_{RWA}}\sqrt{H_X^2(0) + H_Y^2(0)} \tag{D5}$$

$$\Omega_{RWA4}(\max) = \Omega_{RWA2}(\max)$$